Interference effects and magnetoresistance oscillations in normal-metal networks:1-weak localization approach

Benoît Douçot, R. Rammal

J. Physique **47** (1986) 973-999 JUIN **1986,** PAGE 973

Classification
Physics Abstracts
71.50 — 71.555 — 72

Interference effects and magnetoresistance oscillations in normal-metal networks : 1-weak localization approach

B. Doucot and R. Rammal

Centre de Recherches sur les Très Basses Températures, CNRS, B.P. 166 X, 38042 Grenoble Cedex, France

(*Reçu le 22 octobre 1985, accepté sous forme définitive le 20 février 1986*)

Résumé. — Nous présentons un formalisme général pour calculer les coefficients de transport dans un réseau de métal normal en régime de localisation faible. Notre approche est illustrée d'abord sur des circuits simples : boucles, échelles, etc. Des expressions compactes de la magnétorésistance d'un réseau régulier infini (carré, nid d'abeilles, ...) sont obtenues. Le cas d'un réseau fractal infini (tamis de Sierpinski) est aussi étudié. On montre que dans le cas général, la correction de localisation faible à la magnétorésistance est donnée par une somme pondérée sur les valeurs propres du problème linéaire sous-jacent. En particulier, on montre l'absence d'une structure fine due aux effets d'interférence entre boucles adjacentes, et ceci par opposition avec les réseaux supraconducteurs. Nos résultats sont en parfait accord avec les mesures récentes de l'oscillation de la magnétorésistance d'un réseau de métal normal.

Abstract. — A general formalism is outlined for the calculation of the transport coefficients of a normal-metal network in the weak-localization regime. Simple circuits such as loops and ladders are used to illustrate our approach. Closed expressions for the magnetoresistance of infinite regular networks (square, honeycomb, ...) are derived. The case of an infinite fractal network (Sierpinski gasket) is also investigated. We show that the localization correction to the magnetoresistance $\Delta R/R$ is given in general by a weighted sum over the eigenvalues of the underlying linear problem. We find in particular that, in contrast with superconducting networks, no fine structure due to interference effects between adjacent loops is expected. The obtained results are shown to agree very well with recent experimental results on the magnetoresistance oscillations in normal-metal networks.

1. Introduction.

Since the prediction [1] of a Bohm-Aharonov-type effect [2] in disordered metals, with half-quantum flux $\phi_0 = hc/2e$, only three groups were able to observe clearly this effect in the following new multiconnected geometries : regular networks [3], ladders and necklaces [4] and more recently in single ring geometry [5]. The original experiment [6], performed on a hollow cylinder, has been repeated by several groups [7]. The magnetoresistance (MR) oscillations observed in these experiments are actually the manifestation of a specific and new interference phenomenon in disordered materials. Indeed, the flux periodicity $2\phi_0 = hc/e$ of Aharonov-Bohm resistance oscillations have been reported [8] on very pure single-crystal cylinders with long mean free paths. The observation of these interference effects with the period ϕ_0 (superconducting quantum flux) is therefore as fundamental as the Little-Parks experiment [9] on superconductors. The physical explanation for the factor of two in the flux period has been given in reference [10] : the interference effect is due to two counterpropagating electron waves, each of which travels fully around the ring. However, this interference effect, obtained originally through an explicit diagram calculation, is really a very general phenomenon in systems with quenched disorder. Indeed, the basic origin must be traced to the enhancement of backscattering during the propagation of waves in randomly inhomogeneous media, where multiple scattering dominates. As long as $\lambda \ll l$ (λ is the wave length and l is the mean free path), the first interference corrections to the wave-field energy-transport equation are controlled by the so-called fan diagrams. This is actually the case of the weak localization regime. The presence of a magnetic field, which couples to the phase of a wave function, is therefore the most natural method to reveal this interference effect.

Given the fundamental aspect of the interference phenomena in disordered systems, it is natural to look at the corresponding corrections in new geome-

tries, like networks, where the recent experiments were performed. The magnitude of the MR oscillations has been calculated only for the hollow cylinder geometry [1] and, to our knowledge, there is no equivalent expression for the general situation. In addition to the relevance of such a calculation for the experimental investigations [3-5], there are at least two additional motivations for our study. First, how is the amplitude of the MR oscillations influenced by the experimental set up ? Second, are there new features of the MR curve in the case of an extended network ? Actually, these effects will be produced by interferences between adjacent loops in the network. For instance, in superconducting networks, such effects were predicted [11] and observed [12] on the fine structure of the upper critical line. Is there a counterpart in the case of normal networks ? In this paper, the first in a series, we report on a general formalism for the calculation of transport coefficients for a normal-metal network of arbitrary shape. Our formulation, illustrated below explicitly on different examples, permits us to answer the above questions and provides explicit expressions for the MR oscillations for an arbitrary network. In the following, we will limit our exposition to localization corrections in the weak-localization regime. Note, however, that corrections due to electron-electron interaction can also be calculated in the framework of the present formulation. A more detailed exposition will be given elsewhere [13].

A short summary of this paper has been presented in reference [14]. Our aim is to present detailed calculations of the MR oscillations using the Cooperon approach [15]. In section 2, we present the basic equations for the localization correction to the conductivity in network geometry. The network equations thus obtained are illustrated in simple cases : loops with or without arms. In particular, the influence of arms and of contact geometry on the MR oscillations is discussed in this section. Similarly, the interference effects in the case of two adjacent loops are explicitly discussed. Section 3 is devoted to the calculation of $\Delta R/R$ in extended geometries : open or closed ladders, necklaces, ..., etc. Infinite regular networks and fractal networks are worked out in section 4, where simple expressions for $\Delta R/R$ are derived for each case. In order to make contact with experiment, the finite width effect of wires and the spin-orbit scattering contribution are investigated in section 5. An explicit comparison with the available experimental results is illustrated at the end of this section. Our results are discussed in section 6, where contact with other approaches is made. Some technical details are given in Appendices A, B and C.

2. Weak localization corrections to the conductivity in network geometry.

The localization correction to the conductivity in the weak-localization regime ($k_F\, l_e \gg 1$) is given in general by the following expression [16] :

$$\Delta\sigma(\mathbf{r}) = -(2/\pi\nu)\, \sigma_0\, C(\mathbf{r}, \mathbf{r}) \qquad (1)$$

where σ_0 is the bulk conductivity of the sample, given by Drude's formula, and ν is the density of states at the Fermi level. The equation for the Cooperon [15], $C(\mathbf{r}, \mathbf{r}')$ in the presence of a magnetic field (vector potential $\mathbf{A}$) is

$$\left\{\left[-i\nabla_r - \frac{2\pi}{\phi_0}\mathbf{A}(\mathbf{r})\right]^2 + L_\varphi^{-2}\right\} C(\mathbf{r}, \mathbf{r}') = (1/\hbar D)\, \delta(\mathbf{r} - \mathbf{r}'). \qquad (2)$$

Here D denotes the electron diffusion coefficient and $L_\varphi = (D\tau_\varphi)^{1/2}$ is the length over which dephasing of the electron wave function results from inelastic processes. In equation (2), L_φ appears as the fundamental length scale in the problem, and has the same status as the coherence length scale ξ_s in Ginzburg-Landau equations [11, 12] for superconductors. In general, equation (2) must be supplied by boundary conditions on the surface of a given sample. In what follows, we shall limit ourselves to the following free boundary condition :

$$\left(\frac{\partial}{\partial n} - i\frac{2\pi}{\phi_0}\mathbf{A}\cdot\mathbf{n}\right) C(\mathbf{r}, \mathbf{r}') = 0 \qquad (3)$$

where $\mathbf{n}$ is the normal unit vector to the sample surface.

It is important to notice that equations (1) and (2) actually correspond to a self-averaged theory, where all traces of randomness are summarized in L_φ (see section 6 for further discussions). In principle, equations (2), (3) can be used to calculate the local correction $\Delta\sigma(\mathbf{r})$ in an arbitrary geometry. This program has been carried out for bulk systems [16] (1, 2 and 3 Dimensions), as well as for semi-infinite geometries [17]. In the general case, we need the expression of the off-diagonal Green function $C(\mathbf{r}, \mathbf{r}')$ giving the response at point $\mathbf{r}$ to a source term located at point $\mathbf{r}'$. However, in the case of multiconnected geometries, equations (2), (3) can lead to heavy calculations, already in the case of simple circuits such as the hollow cylinder or single rings [1]. In order to go beyond these simple cases, a simplified formalism is of order. This is the object of this section. As will be shown below, the new formulation allows us to follow the influence of multiconnectedness on $\Delta\sigma(\mathbf{r})$ and particularly in the presence of an applied magnetic field.

2.1 WIRE APPROXIMATION AND NETWORK EQUATIONS. — In the following, we will consider networks made of metallic wires, of width and thickness smaller than L_φ. In this limit, the transverse modes of the Cooperon can be neglected, and one recovers a 1 D problem on each wire. Note that the weak-localization approach used here makes sense only if the transverse dimensions of wires are greater than the elastic mean free

path l_e. These two conditions are actually fulfilled in the experiments done on networks [3-5]. The finite width of wires can, however, be taken into account, and this results in a renormalization of L_φ which becomes a function of the magnetic field (see Sect. 5). Note further that this formalism may break down in very small systems [18] where there is a lack of self-averaging of the theory.

Assume, in equation (1), that the position of the source $\mathbf{r}'$ is given and let us denote by $\tilde{C}(\mathbf{r}) \equiv C(\mathbf{r}, \mathbf{r}')$ the corresponding solution of equations (1), (2). Using the notations of figure 1a, $\tilde{C}(\mathbf{r})$ can be written as

$$\tilde{C}(\mathbf{r}) = g(s) \exp\left(i \frac{2\pi}{\phi_0} \int_0^M \mathbf{A} \cdot \mathbf{dl} \right) \tag{4}$$

where the circulation of the vector potential $\mathbf{A}$ is taken along the strand, and $g(s)$ is an unknown function. In the framework of the wire approximation

$$\mathbf{t} \cdot \left(- i\nabla_\mathbf{r} - \frac{2\pi}{\phi_0} \mathbf{A}(\mathbf{r}) \right) \tilde{C}(\mathbf{r}) = $$

$$= - i \frac{dg}{ds} \exp\left(i \frac{2\pi}{\phi_0} \int_0^M \mathbf{A} \cdot \mathbf{dl} \right) \tag{5}$$

and then equation (1) reduces to

$$- \frac{d^2 g}{ds^2} + L_\varphi^{-2} g = 0 . \tag{6}$$

This gives, for points M between two given points α and β, the following solution

$$g(s) = g_\alpha \cosh(s/L_\varphi) + (g_\beta - g_\alpha \cosh(l_{\alpha\beta}/L_\varphi)) \times$$
$$\times \sinh(s/L_\varphi)/\sinh(l_{\alpha\beta}/L_\varphi) . \tag{7}$$

Here $l_{\alpha\beta}$ denotes the length of the strand between α and β.

The complete solution of equations (1), (2) in a network geometry can then be deduced from the expressions of g_α's at nodes. In this respect, equation (7) must be supplemented by a Kirchoff-type equation at nodes. Such an equation is implied by the continuity conditions of C's at nodes (i.e. current conservation law) and can be written as

$$\sum_\beta \left(- i \frac{\partial}{\partial s} \right)_\alpha g = (i/\hbar DS)\, \delta_{r,\alpha} . \tag{8}$$

Here, the sum is taken over nodes β connected to a given node α and the derivative is taken along the corresponding strand (S denotes the cross-section of wires). Note that the boundary condition of equation (3) is nothing else than equation (8), taken at the free end of a strand. In this respect, equation (8) holds in general, without reference to equation (3). Note also that equation (3) can be replaced by other boundary conditions, such as perfect contact ($C(\mathbf{r}, \mathbf{r}') = 0$) points.

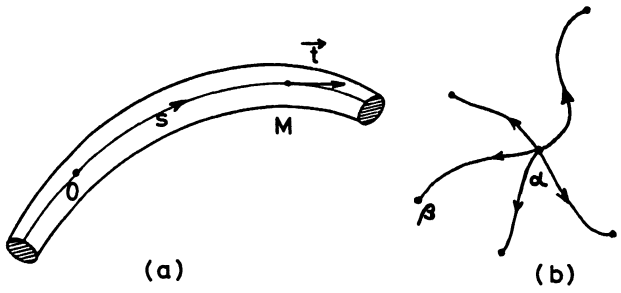

Fig. 1. — (a) A single strand of cross section S, in a normal network. Here s denotes the curvilinear coordinate of point M on the wire : $\mathbf{OM} = \mathbf{r}$ and $\mathrm{OM} = s$. The unit vector $\mathbf{t}$ refers to the tangential vector at point M along the wire. (b) Junction at node α of different strands ($\alpha\beta$) in a part of the network.

It appears from equation (8), that the source point $\mathbf{r}'$ can be considered as an additional node in the network and equations (7), (8) lead to the following network equations

$$\tilde{C}_\alpha \sum_\beta \coth(l_{\alpha\beta}/L_\varphi) - \sum_\beta \tilde{C}_\beta \times$$
$$\times \mathrm{e}^{-i\gamma_{\alpha\beta}}/\sinh(l_{\alpha\beta}/L_\varphi) = (L_\varphi/\hbar DS)\, \delta_{\alpha,\mathbf{r}'} . \tag{9}$$

In equation (9), $\gamma_{\alpha\beta} = \dfrac{2\pi}{\phi_0} \displaystyle\int_\alpha^\beta \mathbf{A} \cdot \mathbf{dl}$, refers to the circulation of the vector potential $\mathbf{A}$ along the strand $\alpha\beta$, of length $l_{\alpha\beta}$, between two nodes α and β (Fig. 1b). Furthermore, the source term at $\mathbf{r}'$, where $\Delta\sigma$ is calculated, acts as an additional node. This remark, as well as other observations, shows the basic differences between equation (9) and the similar one derived for superconducting networks [11].

In principle, equation (9) provides the basic equation for the calculation of $\Delta\sigma(\mathbf{r}')$ at any point $\mathbf{r}'$ and for an arbitrary geometry. In what follows, we shall illustrate these calculations for simple geometries.

2.2 Examples.

2.2.1 *Single wire* (Fig. 2). — Consider a single wire, of length L, $0 \leqslant x \leqslant L$. In this case, equation (9) written for the two nodes $x = 0$, L and for a current node located in between, leads to a system of three linear equations :

$$C(x)\,[\coth(x/L_\varphi) + \coth((L-x)/L_\varphi)] -$$
$$- C(0)/\sinh(x/L_\varphi)$$
$$- C(L)/\sinh\left(\frac{L-x}{L_\varphi}\right) = (L_\varphi/\hbar DS) \tag{10a}$$

$$C(x)/\sinh(x/L_\varphi) - C(0).\coth(x/L_\varphi) = 0 \tag{10b}$$

$$C(x)/\sinh\left(\frac{L-x}{L_\varphi}\right) - C(L) \cdot \coth\frac{L-x}{L_\varphi} = 0. \tag{10c}$$

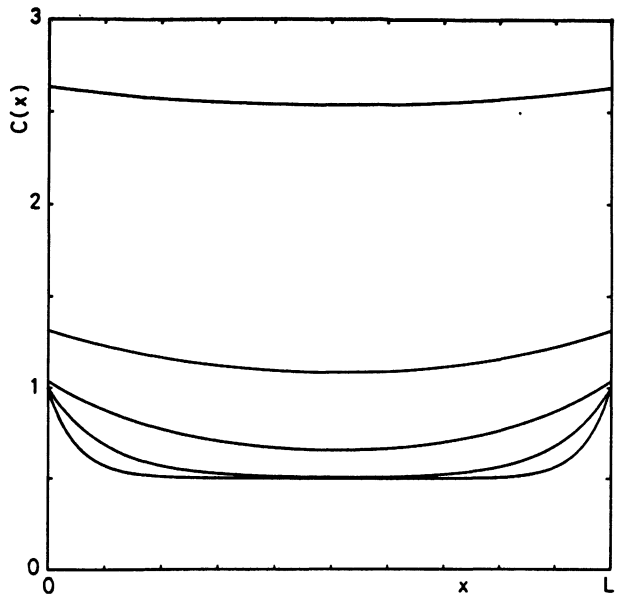

Fig. 2. — Spatial variation of the local localization correction $C(x, x) \sim \Delta\sigma(x)$ to the conductivity of a single wire of length L, equation (12), for $L/L_\varphi = 0.4$, 1, 2, 5 and 10 respectively. $C(x)$ increases as L_φ/L increases, for fixed L.

One deduce from equations (10) the following solution

$$C(x) = \left(\frac{L_\varphi}{\hbar DS}\right) \cosh \frac{x}{L_\varphi} \cosh \frac{L - x}{L_\varphi} \Big/ \sinh (L/L_\varphi) \quad (11)$$

shown in figure 2. $C(x)$ assumes its minimal value at the mid-point $x = L/2$, and takes its maximal value at the ends of the wire ($x = 0$, L). Such a behaviour is actually a very general one : the backscattering corrections to σ are, in general, depressed at points of high coordination number (e.g. $x = L/2$). This remark becomes clearer on the next examples.

Note that the expression (Eq. (11)) found for $C(x)$ is modified when other boundary conditions are used. For instance, if the contact points at the ends are perfect : $C(0) = C(L) = 0$, equations (10) yield :

$$C(x) = \left(\frac{L_\varphi}{\hbar DS}\right) \sinh\left(\frac{x}{L_\varphi}\right) \sinh\left(\frac{L - x}{L_\varphi}\right) \Big/ \sinh (L/L_\varphi) \quad (12)$$

instead of equation (11). In the following, we shall limit our investigation to free boundary conditions (Eq. (3)). In particular, from equation (11), one deduces the integrated correction ΔR to the total resistance of the wire

$$\Delta R = \frac{1}{S} \int_0^L dx\, \Delta(1/\sigma(x)) . \quad (13)$$

Here $\Delta\sigma(x)$ is the local correction given by equation (1). In general $\Delta\sigma(x) \ll \sigma_0$ is a small correction, and equations (11), (13) give

$$\Delta R/R = \frac{\kappa}{2} [\coth (L/L_\varphi) + L_\varphi/L] \quad (14)$$

where we have introduced the dimensionless factor κ :

$$\kappa \equiv \frac{2 e^2 L_\varphi}{\pi\hbar \sigma_0 S} \quad (15)$$

($R = L/\sigma_0 S$).

Equation (14) exhibits the two interesting limits of the wire. The first corresponds to $L/L_\varphi \ll 1$, $\Delta R/R \sim L_\varphi/L$ where ΔR is independent of the wire length L : zero effective dimensionality. The second one is the classical Ohm's law : $\Delta R/R \sim \kappa/2$, recovered at $L/L_\varphi \gg 1$.

Note that for $L \ll L_\varphi$, our result differs from the known one [19] : $\Delta R/R = \frac{\kappa}{2}\left(\coth\left(\frac{L}{L_\varphi}\right) - \frac{L_\varphi}{L}\right)$. The net difference comes from the boundary conditions. Indeed, using equation (12), instead of equation (11), one gets the usual result.

2.2.2 *Single wire with dangling side branches* (Fig. 3a). — The local character of $\Delta\sigma(x)$ is clearly visible in the case of a single wire, when N dangling side branches are attached to it. The compact expression of $\Delta\sigma(x)$ for this geometry is given in Appendix A. In figure 3b, the spatial variations of $C(x, x)$ along the strand are shown, for typical values of a/L_φ and b/L_φ, and for $N = 12$. For non vanishing values of b, the localization correction is modulated with a net depression of $C(x, x)$ at junctions. Two general features are to be noticed, regarding the shape and the amplitude of the modulation. Side branches are responsible for the strong modifications of $C(x, x)$ in the limit $a/L_\varphi \gg 1$, whereas the zero dimension behaviour $a/L_\varphi \ll 1$ is slightly affected. In both cases, the net effect of arms saturates at $b \gg L_\varphi$. Therefore, starting from the single wire behaviour at $b = 0$ (Fig. 2), small and smooth modulations appear near the middle of the wire. Increasing b gives rise to sharper and sharper oscillations of $C(x, x)$ over the whole range of the wire. The magnitude of oscillations increase monotonically with the ratio b/L_φ.

2.2.3 *Single loop in a normal magnetic field* (Fig. 4). — In this geometry, the source position $\mathbf{r}'$ is arbitrary, and equation (9) reduces to

$$\left[-2 \coth (L/L_\varphi) + 2 \cos\left(2\pi \frac{\phi}{\phi_0}\right) \Big/ \sinh (L/L_\varphi)\right] \times C(\mathbf{r}', \mathbf{r}') = -L_\varphi/\hbar DS . \quad (16)$$

Here L denotes the length of the loop and ϕ is the magnetic flux through its surface. Equation (16) leads

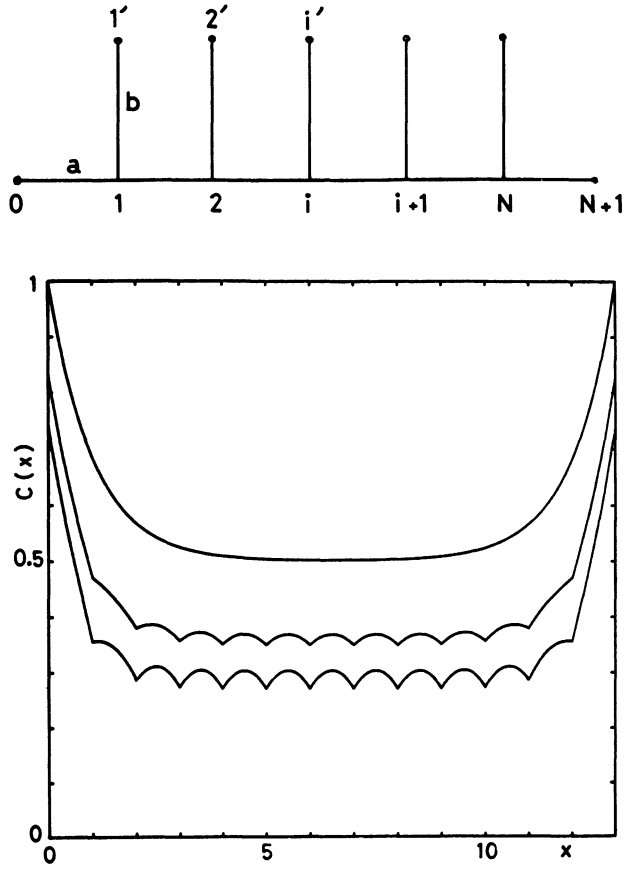

Fig. 3. — (a) A single wire geometry with dandling side branches. (b) The dimensionless local correction to the conductivity as a function of x along the wire. The modulation of $C(x)$ along the wire corresponds to the attenuation of backscattering corrections at junctions of large coordination number ($z = 3$). Here $N = 12$, $a/L_\varphi = 0.5$ and $b/L_\varphi = 0.05$ and 10 respectively. $C(x)$ decreases as b increases.

to

$$C(\mathbf{r}', \mathbf{r}') = \frac{L_\varphi}{2\,\hbar DS} \sinh(L/L_\varphi)/ [\cosh(L/L_\varphi) - \cos(2\,\pi\phi/\phi_0)] \quad (17)$$

reproducing the result of reference [1] in a somewhat elementary way. From equation (17), it is easy to deduce the following expression for the resistance correction $\Delta R/R$, between two opposite points on the loop :

$$\Delta R/R = \frac{\kappa}{2} \sinh(L/L_\varphi)/[\cosh(L/L_\varphi) - \cos(2\,\pi\phi/\phi_0)]. \quad (18)$$

As expected, $\Delta R/R$ exhibits a periodic behaviour in the reduced flux ϕ/ϕ_0. The amplitude of oscillation is $\sim 1/\sinh(L/L_\varphi)$ and then exponentially damped at $L \gg L_\varphi$. In the limit $L/L_\varphi \equiv \eta \ll 1$, one obtains : $\Delta R/R = \kappa/\eta$ at zero field and the width of the maxima

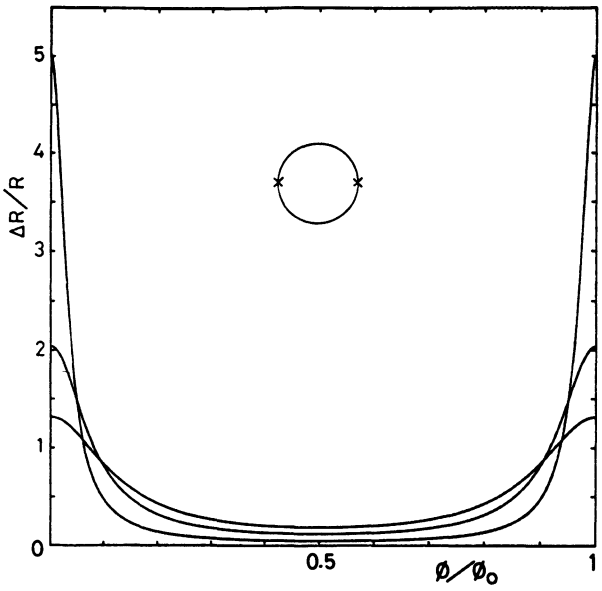

Fig. 4. — Variation of the relative correction $\Delta R/R$ measured in unit of κ (Eq. (15)) between two opposite points A and B on a single ring of circumference L, as a function of the reduced flux $f = \phi/\phi_0$ ($\eta \equiv L/L_\varphi = 0.2$, 0.5 and 0.8 respectively). The maximum of $\Delta R/R$ at integer values of f becomes sharper for smaller η.

at integer ϕ/ϕ_0 is of order of η (sharp maxima). On the other hand, for $\phi/\phi_0 = 1/2$ one obtains $\Delta R/R \sim \eta$, which appears to be quite general : all the networks we studied actually show this behaviour. Note however that at small ϕ/ϕ_0, the single loop exhibits the sharpest behaviour among all networks. Indeed, in more complex geometries (loop with arms, strips, etc.) $\Delta R/R$ at zero field increases more slowly than $1/\eta$ as η goes to zero and the width of the maxima is actually greater than η. The origin of this behaviour must be found in the exponential damping of the Cooperon $C(\mathbf{r}, \mathbf{r}')$, equation (7), over the length scale L_φ. In this respect, the single loop geometry is a useful reference for further comparisons.

2.3 Effect of arms on the resistance oscillations. — Usually the resistance of a ring is measured through two arms attached to it [5]. In the following we shall investigate the influence of such arms on the localization correction to the measured resistance.

2.3.1 *Single ring with one arm* (Fig. 5a). — Using equation (9), it is not difficult to obtain the following expressions for the Cooperon $C(x)$ according to the position of the source node. For M located on the arm, one finds

$$C(x) = \frac{L_\varphi}{\hbar DS}\left[\sinh\frac{L}{L_\varphi}\cosh\frac{x}{L_\varphi}\cosh\frac{b-x}{L_\varphi} + 2\left(\cosh\frac{L}{L_\varphi} - \cos 2\,\pi\frac{\phi}{\phi_0}\right)\cosh\frac{x}{L_\varphi}\sinh\frac{b-x}{L_\varphi}\right]\Big/\Delta \quad (19)$$

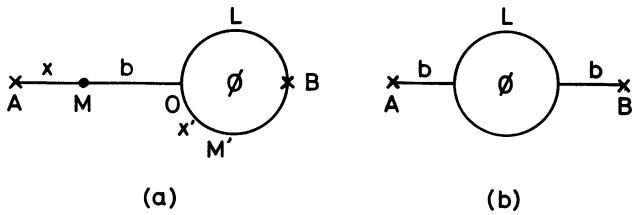

Fig. 5. — (a) A single ring geometry with one arm. ΔR is measured between A and B. (b) A single ring geometry with two arms.

where

$$\Delta = \sinh\frac{b}{L_\varphi}\sinh\frac{L}{L_\varphi} + \\ + 2\cosh\frac{b}{L_\varphi}\left(\cosh\frac{L}{L_\varphi} - \cos 2\pi\frac{\phi}{\phi_0}\right).$$

Similarly, for M′ on the loop, one finds

$$C(x') = \frac{L_\varphi}{\hbar DS}\left[\sinh\frac{b}{L_\varphi}\sinh\frac{x'}{L_\varphi}\sinh\frac{L-x'}{L_\varphi} + \right. \\ \left. + \cosh\frac{b}{L_\varphi}\sinh\frac{L}{L_\varphi}\right]\Big/\Delta . \quad (20)$$

Note that $C(x)$, as given by equation (19), assumes its maximal value at $x = 0$, i.e. at the free end of the arm (point A in Fig. 5a). Similarly, $C(x' = 0)$ is smaller than $C(x' = L/2)$ corresponding to point B. This result agrees with our previous remarks on the depression of C at junction nodes of large coordination numbers. Using equations (19)-(20), it is not difficult to deduce the integrated correction to the resistance R_{AB} measured between points A and B. One gets

$$\Delta R_{AB}/R_{AB} = \kappa\frac{1}{2b + L}\left\{(b\cosh b + \sinh b)\sinh L + 2b\sinh b\left(\cosh L - \cos 2\pi\frac{\phi}{\phi_0}\right) + \right. \\ \left. + L\cosh b\sinh L + \frac{1}{2}\sinh b(L\cosh L - \sinh L)\right\}\Big/\Delta . \quad (21)$$

For convenience, we have replaced b/L_φ and L/L_φ by b and L respectively (b = arm length, L = loop length). The previously obtained results (Eqs. (14), (18)) are recovered for $L = 0$ and $b = 0$ respectively. Furthermore, $\Delta R_{AB}/R_{AB}$ exhibits the expected oscillations as for the single loop. However the magnitude of the oscillations is affected by the presence of the arm. Indeed, for $L \sim b \leqslant L_\varphi$, the correction along the arm (Eq. (19)) and that along the loop (Eq. (20)) become comparable. More precisely, if η denotes the smallest ratio b/L_φ or L/L_φ, then $C(x) \sim 1/\eta$ at $\phi/\phi_0 \sim 0$ and $C(x) \sim \eta$ elsewhere, and this either on the arm or on the loop. In this limit, the maximal correction ΔR_{AB} takes place at $\phi \ll \phi_0$, with a width of order η.

The presence of the arm becomes more and more interesting in the limit $L \ll L_\varphi < b$. In such a case the oscillations are still present because of $L \ll L_\varphi$. However, from equation (20), $C(x)$ becomes independent of η at small $\eta = L/L_\varphi$ for $\phi/\phi_0 \sim 0$ but $C(x) \sim \eta$ for $\phi/\phi_0 \geqslant \eta^{1/2}$. This new behaviour contrasts sharply with the η^{-1} regime found in the absence of the arm. This leads to a damping of the resistance oscillation, when compared with the $b = 0$ case. Furthermore, the sharp maxima at integer values of ϕ/ϕ_0 are broadened by the presence of the arm.

2.3.2 *Single ring with two arms* (Fig. 5b). — The same calculations can be carried out in the case of two arms attached to the loop, as shown in figure 5b. The expression of $\Delta R_{AB}/R_{AB}$ is given by

$$\Delta R_{AB}/R_{AB} = \frac{\kappa}{4b + \frac{L}{2}}\left\{(b + \tanh b)\left(2\cosh\frac{L}{2} + \sinh\frac{L}{2}\tanh b\right)\sinh\frac{L}{2} + \right. \\ + b\tanh b\left[\sinh L\tanh b + 2\left(\cosh L - \cos 2\pi\frac{\phi}{\phi_0}\right)\right] \\ \left. + \frac{1}{4}\left[L\sinh L + (L\cosh L - \sinh L)\tanh b + \left(\frac{L}{2}\cosh\frac{L}{2} - \sinh\frac{L}{2}\right)\sinh\frac{L}{2}\tanh^2 b\right]\right\}\Big/\Delta . \quad (22)$$

Here, Δ is given by

$$\Delta = \cosh L - \cos 2\pi\frac{\phi}{\phi_0} + \sinh L\tanh b + \frac{1}{2}\sinh^2\frac{L}{2}\tanh^2 b . \quad (23)$$

The variations of $\Delta R/R$ as functions of the reduced flux ϕ/ϕ_0 for different values of b/L_φ and L/L_φ are shown in figure 6. The qualitative results found above for one arm, hold also in the present case.

2.3.3 *Two-loop geometries.* — Given the oscillations of the resistance with magnetic field, it is natural to ask for interference effects for two adjacent loops enclosing different magnetic fluxes. For this, it is useful to consider the simple geometries shown in figure 7.

2.3.3.1 Two articulated loops (Fig. 7a). — Using equation (9), it is not difficult to calculate the Cooperon at point x, as shown in figure 7a :

$$C(x) = \frac{L_\varphi}{2\hbar DS}\left[\sinh L_1 \sinh L_2 + 2\left(\cosh L_2 - \cos 2\pi\frac{\phi_2}{\phi_0}\right)\sinh x \sinh (L_1 - x)\right]\Big/\Delta . \tag{24}$$

Here, the denominator Δ is given by

$$\Delta = \sinh L_1.(\cosh L_2 - \cos 2\pi\phi_2/\phi_0) + \sinh L_2(\cosh L_1 - \cos 2\pi\phi_1/\phi_0) . \tag{25}$$

In equations (24), (25), L_i and ϕ_i ($i = 1, 2$) denote respectively the length (divided by L_φ) and the enclosed magnetic flux associated to the loop i. The corresponding integrated correction to the resistance between A and B, can be written as

$$\Delta R_{AB}/R_{AB} = \frac{\kappa}{2}\frac{1}{L_1 + L_2}\left[(L_1 + L_2)\sinh L_1 \sinh L_2 + (L_1 \cosh L_1 - \sinh L_1)\left(\cosh L_2 - \cos 2\pi\frac{\phi_2}{\phi_0}\right) + \right.$$
$$\left. + (L_2 \cosh L_2 - \sinh L_2)\left(\cosh L_1 - \cos 2\pi\frac{\phi_1}{\phi}\right)\right]\Big/\Delta . \tag{26}$$

As it should be, the single loop result (Eq. (18)) is recovered for $L_i = 0$ and $\phi_i = 0$ ($i = 1$ or 2). In general, equation (26) shows the presence of two periodic contributions. For rational ϕ_1/ϕ_2, a periodic behaviour is obtained (Fig. 8a). The resulting period is fixed by the smallest flux. On the contrary, for irrational ϕ_1/ϕ_2 no strictly periodic behaviour is observed, but some sharp maxima can appear in the limit where both ϕ_1/ϕ_0 and ϕ_2/ϕ_0 are very close to integer values. This resonance-like behaviour is illustrated in figure 8b.

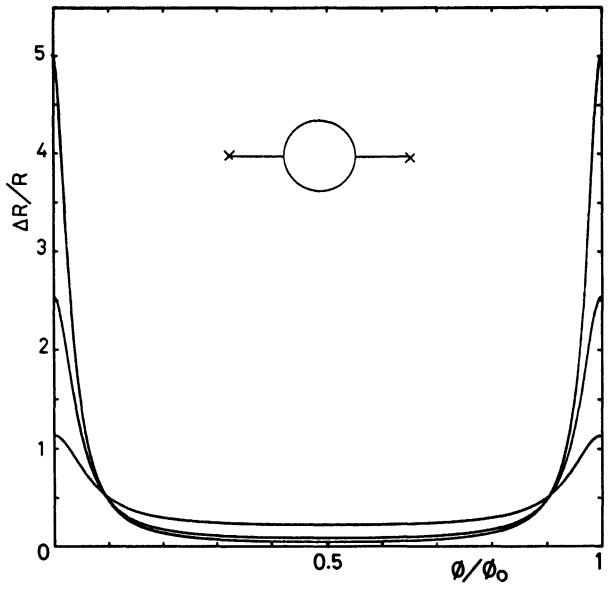

Fig. 6. — $\Delta R_{AB}/R_{AB}$ in unit of κ as a function of the reduced flux ϕ/ϕ_0. The length of the loop is kept fixed at $L/L_\varphi = 0.2$. The length of the arms is gradually increased : $b/L_\varphi = 0$; 0.5; 2.0 and this leads to a net damping of the resistance oscillations.

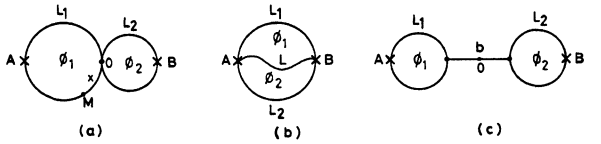

Fig. 7. — Different ways of connecting two loops. (a) two articulated loops; (b) two adjacent loops; (c) two rings with one arm. Here the resistance is measured between points A and B and ϕ_i and L_i correspond to loop i ($i = 1, 2$).

It is important to notice that, for two identical loops ($\phi_1 = \phi_2 \equiv \phi$), no secondary maxima at $\phi/\phi_0 = 1/2$ are obtained. The corresponding behaviour is depicted in figure 9. At first sight this result may appear to be paradoxical. Indeed, on the basis of a naive intuitive argument, new features of $\Delta R/R$ can be expected to occur because of interference effects between adjacent loops. The absence of a new period in the present case must be attributed to the « weak coupling » between the two loops. As will be shown below, a new structure of $\Delta R/R$ may be found in the « strong-coupling » limit.

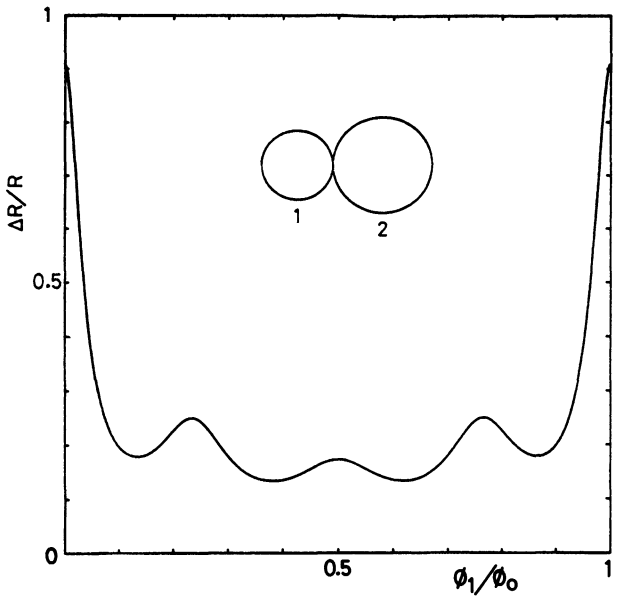

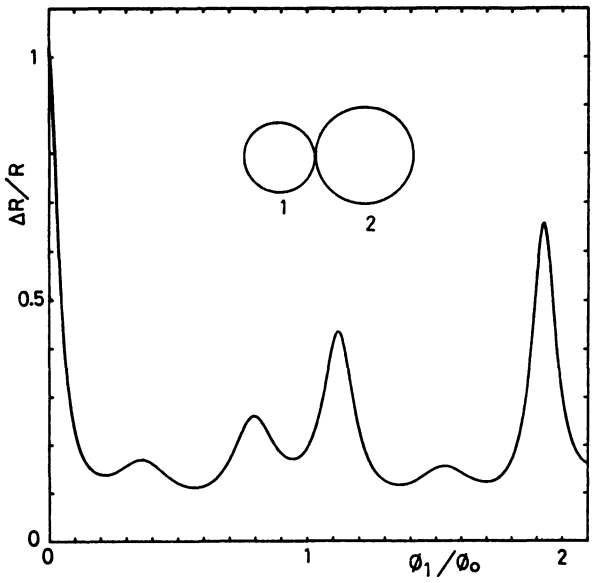

Fig. 8. — (a) $\Delta R_{AB}/R_{AB}$ in units of κ for the system shown on figure 7a, as a function of reduced flux through the smallest loop, which control the period of oscillations. Here $L_1/L_\varphi = 0.4$ and $L_2/L_\varphi = 0.8$. (b) The same plot as in figure 8a but with $L_1/L_\varphi = 0.4$ and $L_2/L_1 = (1 + \sqrt{5})/2$ the golden mean. The non periodic behaviour is due to the non commensurability of the length ratio L_1/L_2.

Note that in the zero dimension limit $L \ll L_\varphi$, equation (26) reduces to the expression corresponding to two identical loops :

$$\Delta R_{AB}/R_{AB} = \frac{\kappa}{4} \sinh (L/L_\varphi)/$$

$$/[\cosh (L/L_\varphi) - \cos (2\pi\phi/\phi_0)]$$

which is exactly equation (18) divided by a factor of 2.

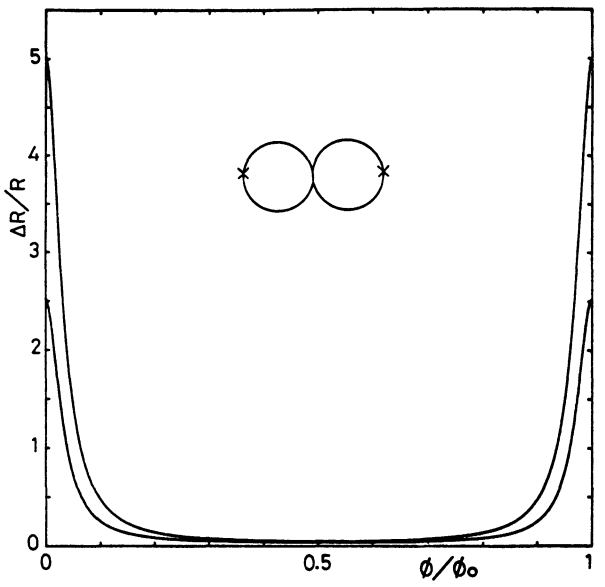

Fig. 9. — $\Delta R/R$ for two identical articulated loops (the lower curve). The upper curve is the result for a single loop of the same size. Note the decrease in the magnitude of the correction when two loops are tied together, as well as the absence of secondary maxima for $\phi/\phi_0 = 1/2$. Here ϕ denotes the magnetic flux through each of the two loops.

This is actually a general property of zero dimensional systems (ΔR is independent of the system size), given the used boundary conditions.

2.3.3.2 Two adjacent loops (Fig. 7b). — A new feature appears in this case, particularly for $L \gg L_1, L_2$ which can be considered as a strong coupling limit between the two adjacent loops. As shown in figure 10, new maxima appear at $\phi/\phi_0 = 1/2$ in the case of two identical loops. This new behaviour, which is absent in the limit $L \sim L_1 \sim L_2$, must be traced to the reduction of the network into a single loop. In fact, because of the strong coupling, the backscattering is inhibited in the long common strand and this holds for arbitrary values of L_φ.

2.3.3.3 Two rings with arms (Fig. 7c). — In addition to the main features found above, an interesting situation appears for two identical loops ($L_1 = L_2 \equiv L$, $\phi_1 = \phi_2 \equiv \phi$) in the zero dimensionality limit $L \ll L_\varphi$. In this case, the local correction is minimal at the middle of the arm (point 0), and this for small values of the reduced flux ϕ/ϕ_0. This is reminiscent to the case of a single wire (Fig. 2), and the presence of loops does not noticeably alter the spatial variation of the local correction on the arm. However, at $\phi/\phi_0 \sim 1/2$, a kind of antibackscattering takes place in the loops, leading to a maximal correction at point 0. This inversion phenomenon can be viewed, in comparison with the single wire case, as an effective modification of the boundary conditions : for small ϕ/ϕ_0, the two loops act as free ends, whereas at half flux, they behave as perfect point contacts.

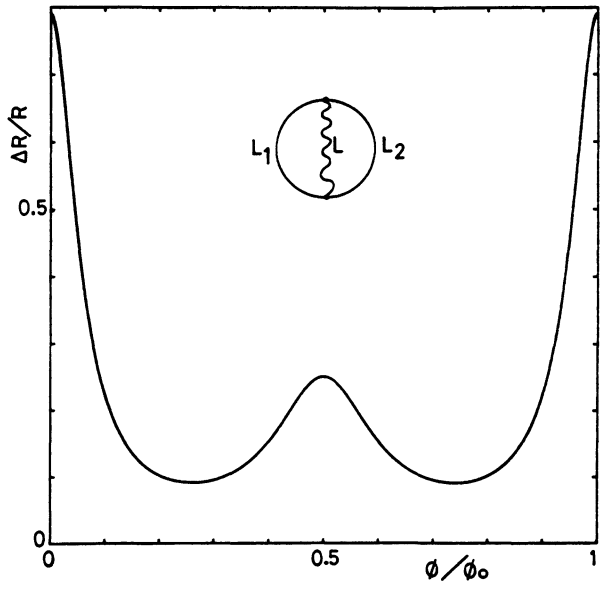

Fig. 10. — $\Delta R_{AB}/R_{AB}$ for two adjacent loops in the « strong coupling limit » $L_1/L_\varphi = L_2/L_\varphi = 0.2$ and $L/L_\varphi = 1.0$. ϕ denotes the magnetic flux across each of the two loops. In this case, a secondary maximum at $\phi/\phi_0 = 1/2$ occurs (compare with Fig. 9).

We have studied other simple geometries, following the same lines of ideas. Some relevant results are summarized in Appendix B. Let us close this section with a few general remarks, which are specific to the backscattering phenomenon in network geometries.

First, the magnitude of the local correction to conductivity, at a given node of the network, decreases when its coordination number increases. This is a very general feature due to the diffusive character of the Cooperon.

Second, the resistance oscillations under an applied magnetic field are damped in the presence of arms. This is also a general feature arising from the inertia of the arms which act as mass terms in the network equations.

Finally, for identical adjacent loops, no new periodic oscillations, coming from interference effects, are expected to occur on $\Delta R/R$. The precise origin of this somewhat puzzling result will become transparent in the next section.

3. General formulation of the magnetoresistance calculation

3.1 BASIC EQUATIONS. — For a given network, with N nodes, we need for the calculation of the Cooperon $C(\mathbf{r}', \mathbf{r})$ the solution of the $(N + 1) \times (N + 1)$ linear system of equation (9). Because of the linearity of equation (9), a somewhat more compact formulation of this problem can be obtained. Let us consider a point $\mathbf{r}'$, along the strand between two nodes α and β (Fig. 11). According to equation (9), one deduces :

$$C(\mathbf{r}', \mathbf{r}) = \frac{L_\varphi}{\hbar D S}\left[\sinh \frac{x}{L_\varphi} \sinh \frac{l_{\alpha\beta} - x}{L_\varphi} \Big/ \sinh \frac{l_{\alpha\beta}}{L_\varphi} + C(\alpha, \mathbf{r}')\, e^{-i\gamma_{\mathbf{r}'\alpha}} \sinh \frac{l_{\alpha\beta} - x}{L_\varphi} \Big/ \sinh \frac{l_{\alpha\beta}}{L_\varphi} + \right.$$

$$\left. + C(\beta, \mathbf{r}')\, e^{-i\gamma_{\mathbf{r}'\beta}} \sinh \frac{x}{L_\varphi} \Big/ \sinh \frac{l_{\alpha\beta}}{L_\varphi}\right]. \quad (27)$$

When (27) is used in (9), written for nodes α and β, one obtains :

$$C(\alpha, \mathbf{r}')\left(\sum_\delta \coth l_{\alpha\delta}/L_\varphi\right) - \sum_\delta \left(e^{-i\gamma_{\alpha\delta}}/\sinh \frac{l_{\alpha\delta}}{L_\varphi}\right) \cdot C(\delta, \mathbf{r}') = \frac{L_\varphi}{\hbar D S} e^{-i\gamma_{\alpha\mathbf{r}'}} \frac{\sinh \dfrac{l_{\alpha\beta} - x}{L_\varphi}}{\sinh \dfrac{l_{\alpha\beta}}{L_\varphi}} \quad (28)$$

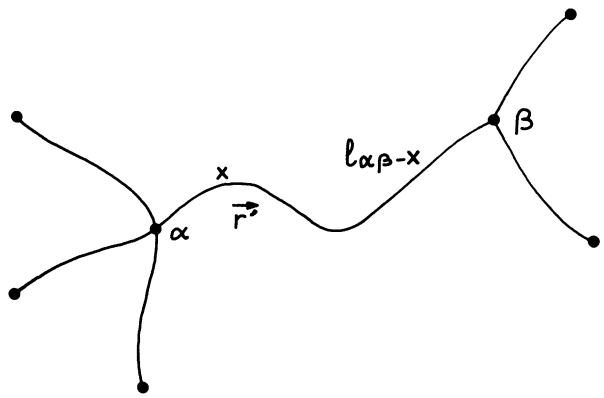

Fig. 11. — A strand $(\alpha\beta)$ on a typical network. $\mathbf{r}'$ denotes the position of the point where $\Delta\sigma$ is calculated and x is its curvilinear coordinate from node α along $(\alpha\beta)$.

as well as a similar equation, obtained by the substitutions : $\alpha \leftrightarrow \beta$, $l_{\alpha\beta} - x \leftrightarrow x$ in equation (28). It is natural to introduce the following Hermitian $N \times N$ matrix M, which is independent of the considered point $\mathbf{r}'$:

$$M_{\alpha\alpha} = \sum_{\beta} \coth (l_{\alpha\beta}/L_\varphi) - 2 \sum_{\text{loops}} \cos (2\pi\phi_s/\phi_0)/\sinh (l_s/L_\varphi) \tag{29a}$$

$$M_{\alpha\beta} = - \exp(- i\gamma_{\alpha\beta})/\sinh (l_{\alpha\beta}/L_\varphi), \qquad \alpha \neq \beta . \tag{29b}$$

In equation (29a), the first sum is taken over nodes β connected to the node α by strands of lengths $l_{\alpha\beta}$. The second sum is taken over the elementary loops, of length l_s, containing the node α and enclosing a magnetic flux ϕ_s.

According to (28), the expressions of $C(\beta, \mathbf{r}')$ and $C(\alpha, \mathbf{r}')$ can be written down using the matrix elements $T_{\alpha\beta}$ of $T = M^{-1}$, the inverse of the matrix M. This leads to the following expression for $C(\mathbf{r}', \mathbf{r}')$:

$$C(\mathbf{r}', \mathbf{r}') = \frac{L_\varphi}{\hbar D S} \left\{ \frac{\sinh x/L_\varphi . \sinh (l_{\alpha\beta} - x)/L_\varphi}{\sinh (l_{\alpha\beta}/L_\varphi)} + \right.$$

$$\left. + \frac{1}{\sinh^2 \dfrac{l_{\alpha\beta}}{L_\varphi}} \cdot \left[T_{\alpha\alpha} \sinh^2 \frac{l_{\alpha\beta} - x}{L_\varphi} + T_{\beta\beta} \sinh^2 \frac{x}{L_\varphi} + 2 \operatorname{Re} (T_{\beta\alpha} e^{-i\gamma_{\alpha\beta}}) \sinh \frac{x}{L_\varphi} \sinh \frac{l_{\alpha\beta} - x}{L_\varphi} \right] \right\} \tag{30}$$

and then to the integrated correction along the strand $(\alpha\beta)$

$$\Delta R_{\alpha\beta}/R_{\alpha\beta} = \frac{\kappa}{2} \frac{L_\varphi}{l_{\alpha\beta}} \left[\left(\frac{l_{\alpha\beta}}{L_\varphi} \cosh \frac{l_{\alpha\beta}}{L_\varphi} - \sinh \frac{l_{\alpha\beta}}{L_\varphi} \right) \left(1 + 2 \operatorname{Re} (T_{\beta\alpha} e^{-i\gamma_{\alpha\beta}})/\sinh \frac{l_{\alpha\beta}}{L_\varphi} \right) \Big/ \sinh \frac{l_{\alpha\beta}}{L_\varphi} + \right.$$

$$\left. + \left(\sinh \frac{l_{\alpha\beta}}{L_\varphi} \cosh \frac{l_{\alpha\beta}}{L_\varphi} - \frac{l_{\alpha\beta}}{L_\varphi} \right) (T_{\alpha\alpha} + T_{\beta\beta})/\sinh^2 \frac{l_{\alpha\beta}}{L_\varphi} \right]. \tag{31}$$

Depending on the specific configuration, used in the measurement of the resistance, the different $\Delta R_{\alpha\beta}$ will be weighted differently, in the calculation of the overall resistance correction ΔR. In what follows, we will choose a uniform weight, which corresponds to the integration of $C(\mathbf{r}', \mathbf{r}')$ over the whole network. The main physical results are not very sensitive to this choice of weights.

3.2 REGULAR NETWORKS. — Assume that all the N_B strands of a regular network have the same length a. The N nodes are assumed to have the same coordination number Z. For such a regular network, one obtains :

$$\frac{\Delta R}{R} = \frac{\kappa}{2} \frac{1}{N_B \eta \sinh \eta} \left[(\eta \cosh \eta - \sinh \eta) \sum_{(\alpha\beta)} \left(1 + \frac{T_{\beta\alpha} e^{-i\gamma_{\alpha\beta}} + T_{\alpha\beta} e^{-i\gamma_{\beta\alpha}}}{\sinh \eta} \right) + \right.$$

$$\left. + (\sinh \eta \cosh \eta - \eta) \sum_{(\alpha\beta)} \left(\frac{T_{\alpha\alpha} + T_{\beta\beta}}{\sinh \eta} \right) \right]. \tag{32}$$

In equation (32), the sums are taken over the $N_B = \frac{1}{2} ZN$ strands of the network ($\eta = a/L_\varphi$). This expression can be simplified further by noting that $M_{\alpha\alpha} = Z \coth \eta$:

$$\Delta R/R = \frac{\kappa}{2} \left[\frac{\eta \cosh \eta - \sinh \eta}{\eta \sinh \eta} \left(1 - \frac{2}{Z} \right) + \frac{2}{N} \sum_{\alpha=1}^{N} T_{\alpha\alpha} \right]. \tag{33}$$

Furthermore, M is Hermitian, of positive eigenvalues λ_i $\left(\text{because of } M_{\alpha\alpha} > \sum_{\beta(\neq\alpha)} | M_{\alpha\beta} | \right)$. Therefore, the final result becomes

$$\frac{\Delta R}{R} = \frac{\kappa}{2} \left[\frac{\eta \cosh \eta - \sinh \eta}{\eta \sinh \eta} \left(1 - \frac{2}{Z} \right) + \frac{2}{N} \sum_{i=1}^{N} \lambda_i^{-1} \right]. \tag{34}$$

This equation shows that the calculation of the magnetoresistance (MR) reduces finally to a trace over the spectrum of the operator M. The result thus obtained can be generalized trivially to the case of node-dependent

coordination numbers Z_α :

$$\frac{\Delta R}{R} = \frac{\kappa}{2}\left[\frac{\eta \cosh \eta - \sinh \eta}{\eta \sinh \eta}\left(1 - \frac{N}{N_B}\right) + \frac{1}{N_B}\sum_{\alpha=1}^{N} Z_\alpha T_{\alpha\alpha}\right]. \tag{35}$$

3.3 EXAMPLES : NECKLACES AND LADDERS.

3.3.1 *Open necklace of loops* (Fig. 12). — Following the notations of figure 12, the non-vanishing elements of the $(N + 1) \times (N + 1)$ matrix M, are given by ($\eta \equiv a/L_\varphi$) :

$$\begin{aligned} M_{1,1} &= 2 \coth \eta\,, \quad M_{N+1,N+1} = 2 \coth \eta \\ M_{\alpha,\alpha} &= 4 \coth \eta\,, \quad (1 < \alpha < N + 1) \\ M_{\alpha,\alpha+1} &= -2 \cos(\pi\phi/\phi_0)/\sinh \eta\,, \quad (1 \leqslant \alpha \leqslant N) \end{aligned} \tag{36}$$

and $M_{\alpha\beta} = M^*_{\beta\alpha}$.

The explicit expression of $\Delta R/R$ is obtained by following the same procedure used as that in Appendix A.

$$\Delta R/R = \frac{\kappa}{2}\left\{\frac{\eta \cosh \eta - \sinh \eta}{\eta \sinh \eta}\,\frac{N-1}{2N} + \frac{1}{2N}\left[\sum_{k=2}^{N} \frac{2 \sinh \eta}{2 \cosh \eta - (V_{k-1} + V_{N-k+1}) \cos \pi\phi/\phi_0}\right] + \frac{1}{N}\frac{\sinh \eta}{\cosh \eta - V_N \cos \pi\phi/\phi_0}\right\}. \tag{37}$$

In equation (37), the sequence $\{ V_k \}$ is defined recursively by :

$$V_1 = \cos(\pi\phi/\phi_0)/\sinh \eta \tag{38a}$$

$$V_{k+1} = \cos(\pi\phi/\phi_0)\Big/\left(2 \cosh \eta - V_k \cos \pi\frac{\phi}{\phi_0}\right). \tag{38b}$$

In the limit $N = \infty$, V_k can be replaced by its limiting value :

$$V_\infty = \left[\cosh \eta - \left(\cosh^2 \eta - \cos^2 \pi\frac{\phi}{\phi_\rho}\right)^{1/2}\right]\Big/\cos \pi\phi/\phi_0\,,$$

and equation (37) reduces to

$$\Delta R/R = \frac{\kappa}{4}\left[\frac{\eta \cosh \eta - \sinh \eta}{\eta \sinh \eta} + \sinh \eta \cdot \left(\cosh^2 \eta - \cos^2 \pi\frac{\phi}{\phi_0}\right)^{-1/2}\right]. \tag{39}$$

The effect of the increasing of N is illustrated in figure 13. Note the absence of fine structure of $\Delta R/R$ in this geometry.

In the case $L_\varphi \ll a$, one would expect that $\Delta R/R$ is the same as for a single loop. Actually it is not true, because a given ring inside the necklace is not described by the same boundary conditions as the single ring considered in section 2.2. Indeed, the whole structure has an influence similar to arms on a given ring, and then a damping of the magnitude of the MR oscillations is actually expected as the number of connected rings increases. This phenomenon can be illustrated by considering the first harmonic of the MR curve, in the $\eta = a/L_\varphi \gg 1$ limit. Indeed, for

a single loop : $$\frac{\Delta R}{R} = \kappa \exp\left(-\frac{L}{L_\varphi}\right) \cos 2\pi\phi/\phi_0$$

two articulated loops : $$\frac{\Delta R}{R} = \frac{\kappa}{2} \exp\left(-\frac{L}{L_\varphi}\right) \cos 2\pi\phi/\phi_0$$

three articulated loops : $$\frac{\Delta R}{R} = \frac{5}{12}\kappa \exp\left(-\frac{L}{L_\varphi}\right) \cos 2\pi\phi/\phi_0$$

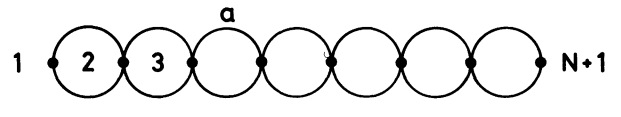

Fig. 12. — An open necklace made of N identical loops, with $N + 1$ nodes. The length of the wire between two nodes is a which is half the length of a loop. We set $\eta = a/L_\varphi$ and ϕ is the magnetic flux through an elementary loop.

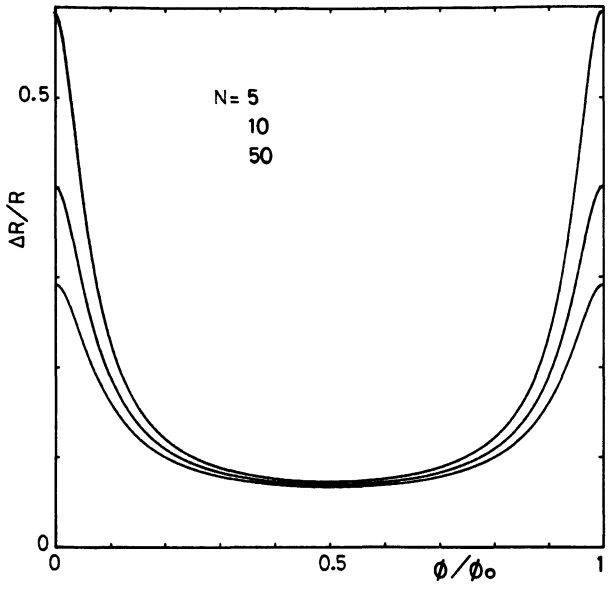

Fig. 13. — $\Delta R/R$ for the necklace of figure 12, in units of κ. The parameters are : $a/L_\varphi = 0.2$ and $N = 5$; 10; 50 respectively. Note that $\Delta R/R$ decreases as N increases as well as the absence of fine structure.

an infinite open necklace : $$\frac{\Delta R}{R} = \frac{\kappa}{4} \exp\left(-\frac{L}{L_\varphi}\right) \cos 2\pi\phi/\phi_0 .$$

Here $L(= 2a)$ denotes the length of elementary loops.

As $\eta \gg 1$, the first harmonic becomes predominant because the backscattering selects only the smallest available loops; then, the functional dependence in ϕ/ϕ_0 is the same for any size of the necklace. However the prefactor decreases as N increases, showing a non-trivial collective effect : the MR oscillations of a given ring are very sensitive to its coupling to the external world, even when L_φ becomes much smaller than its size.

3.3.2 *Closed necklace* (Fig. 14a). — This geometry is worth studying because it will help us to understand the behaviour of a single ring, with finite width. Let us denote ϕ the magnetic flux through each of the N loops and ψ

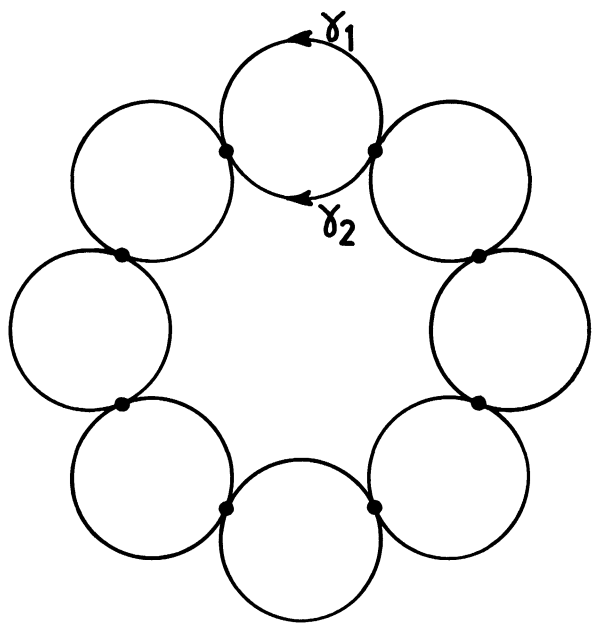

Fig. 14a. — A closed Necklace. γ_1 (resp. γ_2) denotes the phase factor along an external (resp. internal) strand of length a. ψ denotes the magnetic flux through the whole structure defined by taking the mean value $\frac{1}{2}\frac{1}{2\pi N}(\gamma_1 + \gamma_2)$.

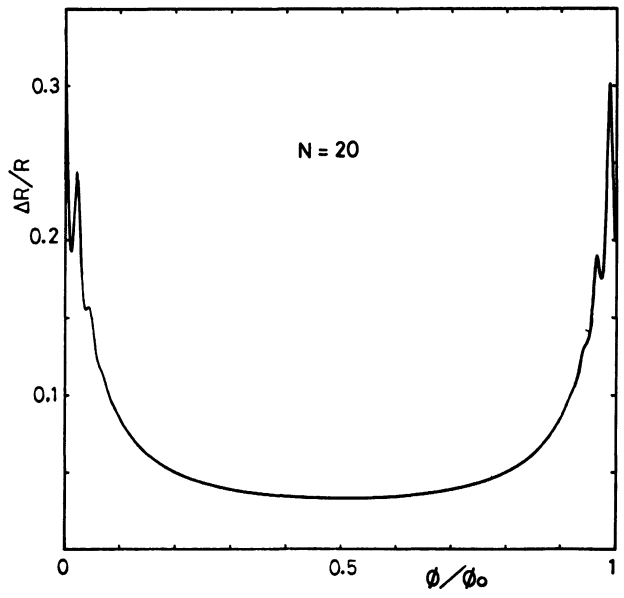

Fig. 14b. — $\Delta R/R$ for a closed necklace of $N = 20$ elementary loops. The elementary loops are located on the circumference of a large ring. Within the main period $0 \leqslant \phi/\phi_0 \leqslant 1$, there are new oscillations due to the presence of the large ring. This system can be viewed as a large ring with a small width simulated by elementary loops. This width is responsible for the attenuation of the oscillations corresponding to the large ring.

the total average flux across the whole network. More precisely

$$\gamma_1 - \gamma_2 = 2\pi\phi/\phi_0\,, \qquad N\gamma_1 = 2\pi\psi_{ext}/\phi_0\,, \qquad N\gamma_2 = 2\pi\psi_{int}/\phi_0$$

and $\psi = \frac{1}{2}(\psi_{ext} + \psi_{int})$.

Due to the rotation symmetry, the eigenvalues λ_k in equation (34) can be easily obtained from the eigenvalue equations :

$$4\cosh\eta . C_n - (e^{-i\gamma_1} + e^{-i\gamma_2}) . C_{n-1} - (e^{i\gamma_1} + e^{i\gamma_2})\, C_{n+1} = \lambda_k \sinh\eta$$

C_n can be taken as $C_n = \alpha_k \exp(2\,i\pi kn/N)$ and then

$$\lambda_k = 4\left[\cosh\eta - \cos\pi\frac{\phi}{\phi_0}\cos\frac{2\pi}{N}(k + \psi/\phi_0)\right]\Big/\sinh\eta \qquad (0 \leqslant k \leqslant N-1). \tag{40}$$

Equation (34) leads to

$$\frac{\Delta R}{R} = \frac{\kappa}{4}\left[\frac{\eta\cosh\eta - \sinh\eta}{\eta\sinh\eta} + \sinh\eta \cdot \frac{1}{N}\sum_{k=1}^{N-1}\left(\cosh\eta - \cos\pi\frac{\phi}{\phi_0}\cos\frac{2\pi}{N}\left(k + \frac{\psi}{\phi_0}\right)\right)^{-1}\right]$$

which can be written as :

$$\frac{\Delta R}{R} = \frac{\kappa}{4}\left[\frac{\eta\cosh\eta - \sinh\eta}{\eta\sinh\eta} + (z_1^N - z_2^N)\sinh\eta\Big/\left(\cosh^2\eta - \cos^2\pi\frac{\phi}{\phi_0}\right)^{1/2} \times \right.$$
$$\left. \times \left(z_1^N + z_2^N - 2\left(\cos\pi\frac{\phi}{\phi_0}\right)^N \cos 2\pi\frac{\psi}{\phi_0}\right)\right]. \tag{41}$$

Here

$$z_{1,2} = \cosh\eta \pm \left(\cosh^2\eta - \cos^2\pi\frac{\phi}{\phi_0}\right)^{1/2}. \tag{42}$$

If the curvature of the ring, in the neighbourhood of an elementary loop, is neglected, one gets $\psi \simeq \frac{N^2}{\pi^2}\phi$. Two limiting procedures are actually of order.

First, one can keep the size of the loops fixed (η fixed) and look at $\Delta R/R$ as a function of ϕ/ϕ_0. In this case, a quasi-periodic modulation is obtained, at $\phi/\phi_0 = n\frac{\pi^2}{N^2}$ (n = integer). Such an interference effect disappears at $Na \gg L_\varphi$ as one could expect. The limit $N = \infty$ reproduces equation (39) relative to the open necklace network. An important difference with the single loop case (parameter 2 η) appears, however in this limit. In fact, for $\phi/\phi_0 \sim 0$ and $\eta \ll 1$, $\Delta R/R$ is no longer of order η^{-1}, but reduces to η^0, whereas the width of the maxima remains of order of η as for the single loop case.

Second, one can keep the network size ηN fixed. In the limit $N = \infty$, we recover the expression $\Delta R/R$ for a single ring with parameter ηN, at least for $\phi/\phi_0 \ll 1$. For finite N, the oscillations characterized by ψ/ϕ_0 = integer are modulated. The envelope and the damping (as ϕ increases) are actually caused by the « penetration » of a non-zero flux ϕ into the elementary loops, leading to a decreasing backscattering in the whole structure. This qualitative picture remains true for a real ring of finite width : the non-zero width is modelled here by the presence of a large number of elementary loops, which take into account the large number of diffusion paths within the width.

3.3.3 *Open ladder* (Fig. 15). — Let $\phi = Ha^2$ be the magnetic flux through each of the N elementary square loops, as shown in figure 15. The inversion of the matrix M can be carried out, following the same iterative procedure described above, where the running variable is now a 2 × 2 matrix. For this, it is useful to define the following matrices :

$$E = \begin{bmatrix} 3\cosh\eta - 1 & 0 \\ 0 & 3\cosh\eta + 1 \end{bmatrix},$$

$$F(\theta) = \begin{bmatrix} \cos\theta & -\sin\theta \\ \sin\theta & \cos\theta \end{bmatrix} \quad (\theta = \pi\phi/\phi_0).$$

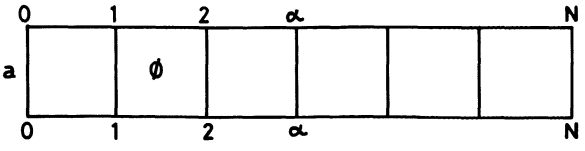

Fig. 15. — A simple open ladder with N elementary loops of side a each ($\eta = a/L_\varphi$).

Two sequences U_i and V_i of 2×2 matrices are defined recursively by :

$$U_i = (E - F(-\phi/\phi_0)\, U_{i-1})^{-1}\, F(\phi/\phi_0), \qquad 1 \leqslant i \leqslant N \tag{43}$$

$$V_i = (E - F(\phi/\phi_0)\, V_{i+1})^{-1}\, F(-\phi/\phi_0), \qquad 0 \leqslant i \leqslant N-1$$

with

$$U_0 = \begin{bmatrix} \cos\theta/(2\cosh a - 1) & -\sin\theta/(2\cosh a - 1) \\ \sin\theta/(2\cosh a + 1) & \cos\theta/(2\cosh a + 1) \end{bmatrix} \tag{44}$$

and V_0 is obtained from U_0 by replacing $\theta = \pi\phi/\phi_0$ by $-\theta$ (here a refers to a/L_φ). Using these notations, the expressions of $T_{\alpha\alpha}$'s to be used in equation (35) are given by

$$T_{\alpha\alpha} = \frac{1}{2}\sinh\eta . \mathrm{Trace}\,[E - F(-\theta)\, U_{\alpha-1} - F(\theta)\, V_{\alpha+1}]^{-1}. \tag{45}$$

This expression holds also for $\alpha = 0$ or N, using the convention $U_{-1} = 0$, $V_{N+1} = 0$ and replacing, in equation (45), E by E' defined by

$$E' = \begin{bmatrix} 2\cosh\eta - 1 & 0 \\ 0 & 2\cosh\eta + 1 \end{bmatrix}.$$

The final result is

$$\Delta R/R = \frac{\kappa}{2}\left[\frac{\eta\cosh\eta - \sinh\eta}{\eta\sinh\eta}\,\frac{N-1}{3N+1} + \frac{2}{3N+1}\left(2\,T_{0,0} + 2\,T_{N,N} + 3\sum_{\alpha=1}^{N-1} T_{\alpha\alpha}\right)\right]. \tag{46}$$

The variations of $\Delta R/R$ as a function of the reduced flux ϕ/ϕ_0 are shown in figure 16.

3.3.4 *Closed ladder* (Fig. 17). — For this geometry, in addition to the principal period, corresponding to ϕ/ϕ_0 integer, secondary oscillations appear at low ϕ/ϕ_0. The number of these oscillations, which are due to the two enclosed fluxes ϕ_1 and ϕ_2 by the internal and external major loops, increases for increasing N, but their magnitude decreases.

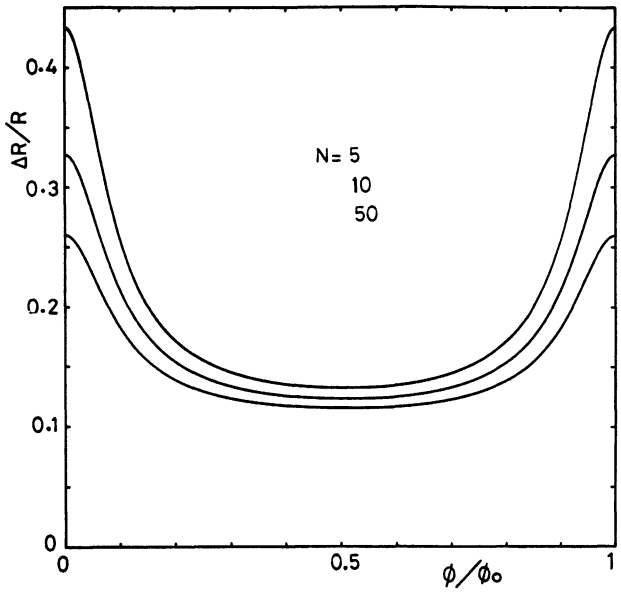

Fig. 16. — $\Delta R/R$ for the open ladder of figure 15. Here $\eta = 0.2$ and N is set equal to 5, 10, 50 respectively. The qualitative features are the same as in the open necklace case (Fig. 13).

4. Infinite regular networks.

In order to study the case of an infinite network, two approaches can be used. The first one is based on equation (34) and the second one is the multistrip approach.

4.1 MULTISTRIP GEOMETRIES (Fig. 18). — In addition to their own interest, multiple strip networks can be used to investigate two limiting problems. The first is the 1D-2D crossover of the magnetoresistance, obtained by increasing the width M of the strip. The second one is the strict limit $M = N = \infty$ of the infinite network.

Let us denote by ϕ the magnetic flux through the elementary square loop. Using the radial gauge, $\mathbf{A} = \frac{1}{2}\,\mathbf{H} \times \mathbf{r}$, the circulation of the vector potential $\mathbf{A}$ is given by $\gamma_m = \left(\frac{N}{2} + 2\pi(m-1)\right)\phi/\phi_0$ at level m. Here N denotes the number of loops in each of the M shells. The solution of equation (35) leads to the following result ($\eta = a/L_\varphi$) :

$$\Delta R/R = \frac{\kappa}{2}\left[\frac{\eta\cosh\eta - \sinh\eta}{\eta\sinh\eta}\,\frac{M-1}{2M-1} + \frac{\sinh\eta}{N(2M-1)}\sum_{k=0}^{N-1}\sum_{m=1}^{M}\frac{4 - \delta_{m,1} - \delta_{m,M}}{E_k(m) - v_k(m-1) - w_k(m+1)}\right]. \tag{47}$$

Here,

$$\begin{aligned} E_k(m) &= 4\cosh\eta - 2\cos(\gamma_m + 2\pi k/N), && 2 \leqslant m \leqslant M-1 \\ &= 3\cosh\eta - 2\cos(\gamma_m + 2\pi k/N), && m = 1 \quad \text{or} \quad M \end{aligned} \tag{48}$$

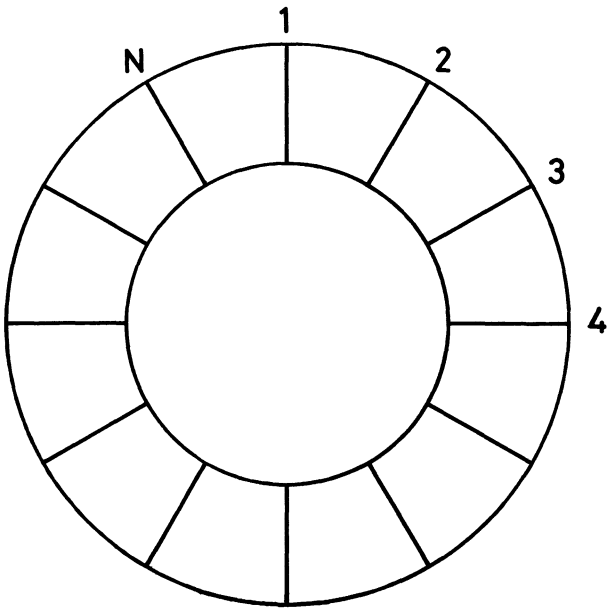

Fig. 17. — A closed ladder geometry with N elementary cells.

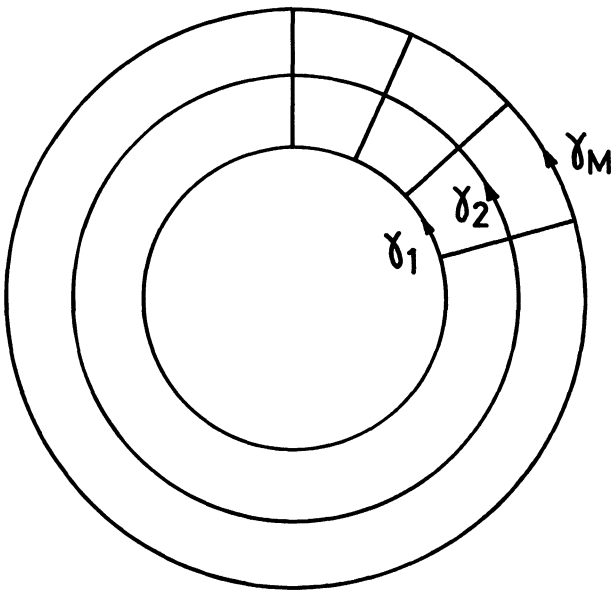

Fig. 18. — A multiple strip geometry. Here ϕ denotes the magnetic flux across an elementary loop and γ_m is the dephasing factor along a strand in a radial gauge. a is the side of an elementary loop. $\eta = a/L_\varphi$.

and

$$\begin{aligned} v_k(1) &= 1/E_k(1), \quad v_k(m) = 1/(E_k(m) - v_k(m-1)) \\ w_k(M) &= 1/E_k(M), \quad w_k(m) = 1/(E_k(m) - w_k(m+1)). \end{aligned} \tag{49}$$

Qualitatively, the behaviour of $\Delta R/R$ is identical to that of the single strip network. Let us just discuss the limit of large N and M. For the sake of clarity, we shall only consider the limit of zero magnetic field $H = 0$. In this case, for finite N, the sequences $v_k(m)$ and $w_k(m)$ converge rapidly to their common limit $v_k(\infty)$ as $M \to \infty$. In this limit, equation (47) becomes

$$\Delta R/R = \frac{\kappa}{4}\left[\frac{\eta \cosh \eta - \sinh \eta}{\eta \sinh \eta} + \sinh \eta \frac{1}{N} \sum_{k=0}^{N-1} \frac{4}{E_k - 2 v_k(\infty)}\right] \tag{50}$$

where E_k denotes the common value of $E_k(m)$ at zero field, related to $v_k(\infty)$ by $E_k - (E_k^2 - 4)^{1/2} = 2 v_k(\infty)$. Taking now the limit $N = \infty$, one obtains :

$$\Delta R/R = \frac{\kappa}{4}\left[\frac{\eta \cosh \eta - \sinh \eta}{\eta \sinh \eta} + \frac{2}{\pi} \sinh \eta \int_0^{2\pi} \frac{dx}{[(4 \cosh \eta - 2 \cos x)^2 - 4]^{1/2}}\right]. \tag{51}$$

The integration in equation (51) can easily be performed, and leads to

$$\Delta R/R = \frac{\kappa}{4}\left[\frac{\eta \cosh \eta - \sinh \eta}{\eta \sinh \eta} + \frac{2}{\pi} \tanh \eta . \mathbb{K}(1/\cosh \eta)\right] \tag{52}$$

where $\mathbb{K}(\ )$ denotes the complete elliptic integral of first kind $\mathbb{K}(k) = \int_0^{\pi/2} dx(1 - k^2 \sin^2 x)^{-1/2}$. The continuum limit of equation (52), given by $\eta = a/L_\varphi \ll 1$, reproduces the 2D bulk behaviour, as it should be. Indeed, for $\eta \ll 1$, $\mathbb{K}(1/\cosh \eta) \simeq \ln(4/\tanh \eta)$ and equation (52) yields

$$\Delta R/R \simeq \frac{\kappa}{2\pi} \frac{a}{L_\varphi} \ln\left(\frac{L_\varphi}{a}\right) \tag{53}$$

$\left(\text{we recall that } \kappa = \frac{2e^2}{\pi \hbar \sigma_0} \frac{L_\varphi}{S}\right)$.

The final expression, equation (53) corresponds to the known one [16] :

$$\Delta R = \frac{e^2}{\pi^2 \hbar} R_{\square}^2 \ln (L_\varphi / l) \qquad (54)$$

where, instead of the elastic mean free path l, the lattice spacing a appears in the network result. The occurrence of a as a short length scale cutoff is actually not surprising. The continuum limit of the network calculation is actually valid up to $a \gtrsim l$. For a lattice spacing $a < l$, the wire approximation breaks down because σ_0 cannot be defined properly in this limit.

4.2 INFINITE SQUARE NETWORK. — The calculation of $\Delta R/R$ can be performed directly, using the result of equation (34) :

$$\Delta R/R = \frac{\kappa}{2}\left[\frac{1}{2}\,\frac{\eta \cosh \eta - \sinh \eta}{\eta \sinh \eta} + \frac{2}{N^2}\sum_{i=1}^{N^2} 1/\lambda_i\right] \qquad (55)$$

where λ_i are the (positive) eigenvalues of the $N^2 \times N^2$ matrix M. Here N^2 is the number of elementary square loops in the network. For large N and finite L_φ, boundary effects can be neglected and one recovers the calculation of the spectrum of matrix M. For convenience, it is useful to take a Landau gauge : $A_x = -Hy$, $A_y = 0$ and $A_z = 0$. Let us denote by $\gamma_m = 2\pi \frac{\phi}{\phi_0} m$ the dephasing factor between nodes (m, n) and $(m, n-1)$ (for the notation, see Fig. 19). The eigenvalue problem, associated to the matrix M, can be written ($\eta = a/L_\varphi$) :

$$(4 \cosh \eta - \lambda \sinh \eta)\, C_{m,n} = e^{-i\gamma_m} C_{m,n-1} + e^{i\gamma_m} C_{m,n+1} + C_{m-1,n} + C_{m+1,n} \qquad (56)$$

(λ refers in Eq. (56) to the eigenvalues of M).

Using the translation symmetry in x direction, one can find the solutions of equation (56), as plane waves in x direction : $\tilde{C}_m e^{ikn}$, $0 \leqslant k \leqslant 2\pi/a$. Therefore, equation (56) reduces to Harper's well-known equation :

$$(4 \cosh \eta - \lambda \sinh \eta)\, \tilde{C}_m = 2 \cos(\gamma_m + ka)\, \tilde{C}_m + \tilde{C}_{m-1} + \tilde{C}_{m+1} \qquad (57)$$

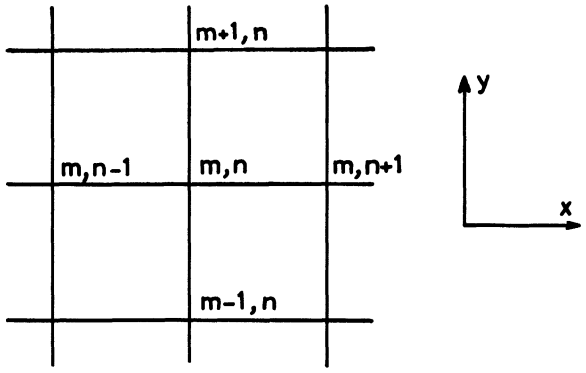

Fig. 19. — Notations for the infinite square network geometry. The side of a loop is denoted by a and $\eta = a/L_\varphi$.

which can also be cast as

$$\varepsilon \psi_m = \psi_{m-1} + \psi_{m+1} + 2 \cos\left(2\pi \frac{\phi}{\phi_0} m + \theta\right) \psi_m \qquad (58)$$

where $\varepsilon = 4 \cosh \eta - \lambda \sinh \eta$ and $\theta = ka$ is a factor of Floquet.

The spectrum of equation (58) has been previously worked out by various authors [20, 21]. The explicit calculation of the eigenvalues ε can be carried out for rational flux $\phi/\phi_0 = p/q$. For these values of the flux, the solution ψ_m can be chosen as $\psi_m = \exp\left(i \frac{m}{q} \varphi\right) . v_m$, where φ denotes a phase factor. Due to the q-periodicity in m direction, one can limit the search for solutions to those such that $v_{m+q} = v_m$. In this way, the eigenvalues ε are given by the solutions of a secular equation : $\det D = 0$, where D is a $q \times q$ Hermitian matrix, of non-vanishing elements :

$$\begin{aligned} D_{l,l} &= 2 \cos\left(2\pi \frac{p}{q} \cdot l + \theta\right) - \varepsilon, \quad 1 \leqslant l \leqslant q \\ D_{l,l+1} &= D_{l+1,l} = 1, \qquad\qquad 1 \leqslant l \leqslant q-1 \\ D_{1,q} &= D_{q,1}^* = \exp(-i\varphi) . \end{aligned}$$

The secular equation actually assumes a very simple form [21] :

$$P_{p,q}(\varepsilon) = 2 \cos \varphi + 2 \cos q\theta \equiv W \qquad (59)$$

where $P_{p,q}(\varepsilon) = \varepsilon^q + \cdots$ is a polynomial of degree q in ε and W is a current variable, $-4 \leqslant W \leqslant 4$. In general, there are q subbands in the spectrum of equation (58), contained in the interval $|\varepsilon| \leqslant 4$, the subband edges are given by : $P_{p,q}(\varepsilon) = \pm 4$. Therefore, equation (55) becomes

$$\Delta R/R = \frac{\kappa}{2}\left[\frac{\eta \cosh \eta - \sinh \eta}{2 \eta \sinh \eta} + \frac{\sinh \eta}{2\pi^2 q}\int_0^{2\pi} d\varphi \int_0^{2\pi} d\mu \sum_{i=1}^{q} (4 \cosh \eta - \varepsilon_i(\varphi, \mu))^{-1}\right] \qquad (60)$$

where $\varepsilon_i(\varphi, \mu)$ refers to the $q (1 \leqslant i \leqslant q)$ subbands and $\mu = q\theta$. Note that $4 \cosh \eta \geqslant 4$ lies outside the spectrum

$| \varepsilon | \leqslant 4$ and the sum in equation (60) is very well behaved. The above result can be simplified further, by performing the sum over the q subbands. Indeed, from equation (59), one deduces

$$\sum_{i=1}^{q} \frac{1}{4 \cosh \eta - \varepsilon_i(\varphi, \mu)} = \frac{P'_{p,q}(4 \cosh \eta)}{P_{p,q}(4 \cosh \eta) - W(\varphi, \mu)}. \tag{61}$$

Furthermore, the integration is quite trivial and leads to the final result

$$\Delta R/R = \frac{\kappa}{4}\left[\frac{\eta \cosh \eta - \sinh \eta}{\eta \sinh \eta} + \frac{8 \sinh \eta}{\pi q} \frac{P'_{p,q}(4 \cosh \eta)}{P_{p,q}(4 \cosh \eta)} \mathbb{K}\left(\frac{4}{P_{p,q}(4 \cosh \eta)}\right)\right]. \tag{62}$$

In equations (61) and (62), $P'_{p,q}$ refers to the derivative of the polynomial $P_{p,q}(\varepsilon)$, defined by equation (59), and taken at $\varepsilon = 4 \cosh \eta$. Note that, because $4 \cosh \eta \geqslant 4$, the argument $k \equiv 4/P_{p,q}(4 \cosh \eta)$ of the complete elliptic integral, lies inside the interval (0, 1) and equation (62) is well defined for all p, q and η. This rather simple and compact expression (Eq. (62)) can then be used to calculate $\Delta R/R$ for arbitrary η and every rational flux p/q. Indeed, one has just to calculate the polynomial $P_{p,q}(\varepsilon)$ and there is no need for further information such as the eigenvalues, the density of states or the ordering of the subbands. Let us mention that in superconducting networks [11-12], it is the edge of the spectrum which is involved. Here, $\Delta R/R$ gives additional spectral information, taking into account the whole structure of the spectrum. This remark is at the origin of the difference between these two problems, although very close to each other. Furthermore, the absence of fine structure in the $\Delta R/R$ curve, has its origin on the expression equation (62) so obtained. In fact, despite the rich structure of the spectrum associated with equation (58), $\Delta R/R$ is given by a regularizing sum (Eq. (55)) over the subbands of this spectrum, weighted by the density of states. Furthermore, equation (62) is analytic, because $4 \cosh \eta$ lies outside the spectrum $| \varepsilon | \leqslant 4$ of equation (55).

Before discussing the numerical results, it is useful to discuss the behaviour of $\Delta R/R$ in some limiting cases.

4.2.1 *Zero field limit.* — For $\phi/\phi_0 = 0$, one can take $q = 1$ and $P(\varepsilon) = \varepsilon$. The eigenvalues are given by $\varepsilon = 2 \cos \varphi + 2 \cos \mu$ and the multistrip result (Eq. (52)) is simply recovered. In this limit as well as for integer ϕ/ϕ_0, one obtains : $\Delta R/R \sim \eta \ln 1/\eta$ at $\eta \ll 1$, to be compared with the single loop behaviour : $\Delta R/R \sim \eta^{-1}$ and the simple ladder one : $\Delta R/R \sim \eta^0$. Therefore, by increasing the effective dimensionality of the network ($d = 0$, 1 and 2), $\Delta R/R$ decreases at zero field and small $\eta = a/L_\varphi$. On the contrary, for non integer values of ϕ/ϕ_0, $\Delta R/R \sim \eta$ in the three cases. A direct comparison is shown in figure 20.

4.2.2 *Small field limit.* — In the limit of vanishing magnetic field, the width of subbands becomes smaller and smaller, giving rise to Landau levels. For instance, at $\phi/\phi_0 = 1/q$, one obtains, close to the lower edge ($\varepsilon = -4$) :

$$\varepsilon = -4 + \left(\frac{1}{2} + n\right)\frac{4\pi}{q}, \quad n = \text{integer}.$$

In this case, the band structure can be well approximated by a central subband $| \varepsilon | < \varepsilon^*$ and a discrete set of Landau levels, with $n \lesssim n^*$ and $n^* \sim q$. Here ε^* and n^* are chosen such as to secure the normalization of the total density of states. Using this approxi-

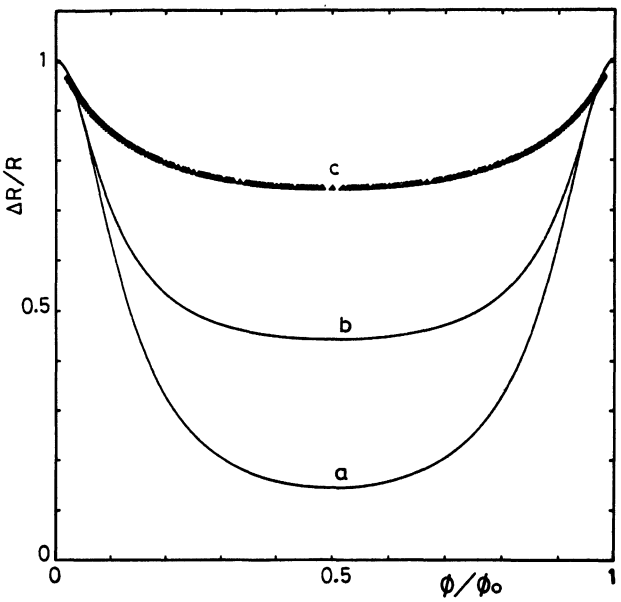

Fig. 20. — $\Delta R/R$ as a function of the reduced flux ϕ/ϕ_0 shown for three networks ($a/L_\varphi = 0.2$) : curve a, single square loop of perimeter $L = 4a$ (Eq. (18)); curve b, simple ladder made of identical square loops, of side a; and curve c, infinite regular network made of identical square loops (Eq. (62)). For convenience, $\Delta R/R$ has been normalized to its value at zero field in each case. Triangles, corresponding to case c, are calculated for rational $\phi/\phi_0 = p/q$, $p < q \leqslant 50$, according to equation (62). Note the absence of fine structure as well as the broadening of the maxima as the effective dimensionality of the network increases.

mation, one obtains :

$$\frac{\Delta R}{R}(H=0) - \frac{\Delta R}{R}(H) \sim \frac{\kappa}{4\pi}\left[\int_{4-\varepsilon^*}^{4} d\varepsilon \frac{8\cosh\eta}{16\cosh^2\eta - \varepsilon^2} - \frac{4\pi}{q}\sum_{n=0}^{n^*} \frac{8\cosh\eta}{16\cosh^2\eta - \left(4 - \frac{4\pi}{q}\left(n+\frac{1}{2}\right)\right)^2}\right]. \tag{63}$$

Note that the integrand in equation (63) has a width $\sim \eta^2$ at $\eta \sim 0$ and $\varepsilon \lesssim 4$. In order to discuss the limiting behaviours of equation (63), it is useful to introduce the magnetic length l_H, defined by : $l_H = a(\phi_0/\phi)^{1/2}$, and giving the spatial extension, in units of a, of a region enclosing one quantum flux ϕ_0.

a) Case $l_H \gg L_\varphi$: In this case, $\eta^2 \gg \phi/\phi_0$ and the difference between the discrete sum and the integral in equation (63) behaves as q^{-2}, i.e. H^2 as expected [16].

b) Case $l_H \ll L_\varphi$: The discrete sum is a poor approximation and this particularly near $\varepsilon = 4$. This is due mainly to the discreteness of the Landau levels, where their relative separation is very large compared to the width $\sim \eta^2$ of the integrand. In this case, the leading contribution is controlled by the singularity at $\varepsilon = 4$ and then

$$\frac{\Delta R}{R}(H=0) - \frac{\Delta R}{R}(H) \simeq \ln(1 + L_\varphi^2/l_H^2) \sim \ln H.$$

Therefore, in both limits, the continuum results [16] for a 2D bulk system are recovered from the network calculations. In figure 20, some results for the infinite square lattice network are shown together with the single loop and the simple ladder results. Here $\phi/\phi_0 = p/q$, with $p < q \leqslant 50$ have been used in the numerical calculation. As was anticipated before, the variation of $\Delta R/R$ as a function of the reduced flux does not exhibit any singularity or fine structure. Only the usual logarithmic singularity arises in the limit of small fields $q \gg 1$ and $\eta \sim 0$. Therefore the results for the infinite network geometry confirm all the characteristic features exhibited by finite networks.

4.3 INFINITE HONEYCOMB NETWORK (Fig. 21). — In principle other infinite regular networks can be studied as above. The main features, found for the square network remain present on the other networks (triangular, honeycomb) : a proper continuum limit, absence of fine structure, etc. In what follows, we shall derive the analogous of equation (62), but for the honeycomb networks where experimental results are available [3]. In this case, the spectrum is also given by a dispersion equation which has the same structure as equation (59). Actually, we have [22] a similar polynomial equation :

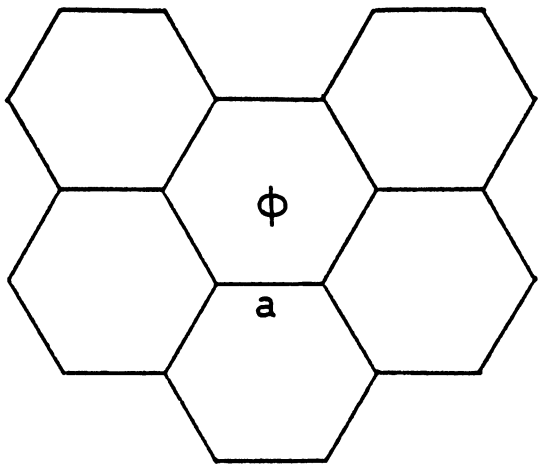

Fig. 21. — A honeycomb network geometry. Here a denotes the length of a strand and ϕ the magnetic flux through a hexagonal elementary cell. $\eta = a/L_\varphi$.

$$P_{p,q}(\varepsilon^2 - 3) + W(\theta_1, \theta_2) = 0 \tag{64}$$

where

$$W(\theta_1, \theta_2) = (-2)^{pq}\cos q\theta_1 + (-1)^{q+1}(2\cos q\theta_2 + 2(-1)^{pq}\cos q(\theta_1 + \theta_2)). \tag{65}$$

For more details, we direct the reader to reference [22]. Note, however that the polynomial in equation (64) is not identical to that used in the square network case. The sum over the spectrum (Eq. (34)) can be cast in the following simple form :

$$\Delta R/R = \frac{\kappa}{6}\left\{\frac{\eta\cosh\eta - \sinh\eta}{\eta\sinh\eta} - \frac{36}{\pi q}\frac{\sinh\eta\cosh\eta . P'_{p,q}(9\cosh^2\eta - 3)}{[A^2 - 12 + 8(3-A)^{1/2}]^{1/2}}\mathbb{K}\left(\frac{4(3-A)^{1/4}}{[A^2 - 12 + 8(3-A)^{1/2}]^{1/2}}\right)\right\}$$

for $A < 0$, and

$$\Delta R/R = \frac{\kappa}{6}\left\{\frac{\eta\cosh\eta - \sinh\eta}{\eta\sinh\eta} + \frac{18}{\pi q}\frac{\sinh\eta\cosh\eta . P'_{p,q}(9\cosh^2\eta - 3)}{(uv)^{1/2}}\mathbb{K}\left(\left(\frac{4-(u-v)^2}{4uv}\right)^{1/2}\right)\right\} \tag{66}$$

for $A > 0$.

Here $A = P_{p,q}(9 \cosh^2 \eta - 3)$ and for $A > 0$, u and v are defined by

$$u = \frac{1}{2}(A^2 + 4A - 12)^{1/2}$$

$$v = \frac{1}{2}(A^2 - 4A + 4)^{1/2}.$$

This expression for $\Delta R/R$ has been used in reference [14] and compared with the experimental data [3]. The agreement was excellent and this will be discussed in section 5.

4.4 INFINITE SELF-SIMILAR NETWORKS (Fig. 22). — It appears now that the magnetoresistance does not exhibit any fine structure in an infinite network geometry. It is then natural to ask whether such a fine structure exists in a self-similar network such as the Sierpinski gasket. In fact, for such a network a whole hierarchy of loops, at all length scales, is present and may favour the appearance of an infinitely countable set of singularities at small magnetic field.

As was shown previously, $\Delta R/R$ is directly related to the tight-binding Hamiltonian, on the underlying network, under an applied magnetic field. This problem has been studied recently by different authors [11, 23, 24], but a compact solution is not yet available. However, the scale invariance of this network allows a recursive calculation of $\Delta R/R$, using equation (34). Actually, the sum in equation (34) is taken at an energy lying outside the spectrum and then $\Delta R/R$ can be obtained numerically after a few iterations. Details are given in Appendix C. Here we shall discuss some limiting cases.

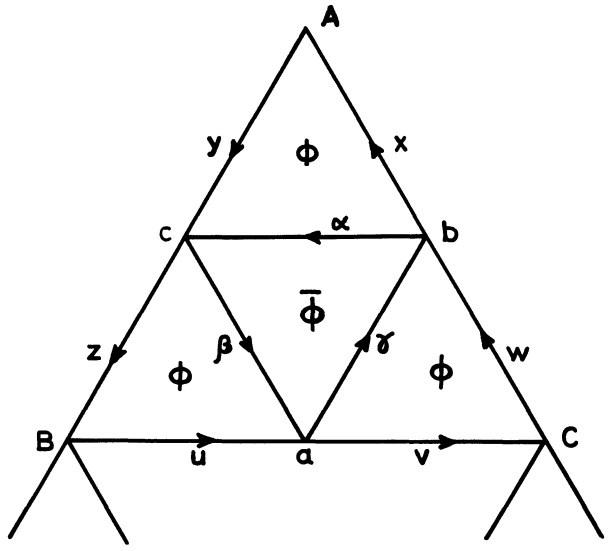

Fig. 22. — A Sierpinski gasket geometry and the corresponding decimation procedure. At a given step, the renormalized magnetic flux is denoted by ϕ, the flux through a corner triangle and $\bar{\phi}$, the flux through a central triangle. Any choice of dephasing factors α, β, γ, μ, ν, ..., z compatible with ϕ and $\bar{\phi}$ can be used. One must imagine that the fractal is infinite, with a finite lowest length scale.

4.4.1 *Zero field limit.* — The expected scaling law for $\Delta R/R$ as a function of the phase breaking time τ_φ, is obtained through an argument, similar to that of reference [25]. One gets :

$$\Delta R/R \sim \tau_\varphi^{(2-\tilde{d})/2} \qquad (\tilde{d} < 2) \tag{67}$$

where $\tilde{d}$ denotes the spectral dimensionality of the structure [26, 27]. However, because of the anomalous diffusion on fractal structure, the definition of the phase coherence length has to be modified. If L_φ denotes the « bare » phase coherence length $L_\varphi = (D\tau_\varphi)^{1/2}$, then the true phase coherence length $\mathfrak{L}_\varphi$ must be defined by

$$\mathfrak{L}_\varphi/a = (L_\varphi/a)^{\tilde{d}/\bar{d}} \tag{68}$$

($\bar{d}$ = fractal dimensionality).

From equations (67), (68), one deduces the following result

$$\Delta R/R \sim L_\varphi^{(2-\tilde{d})} \sim \mathfrak{L}_\varphi^{-\beta_L} \tag{69}$$

where $-\beta_L = (2 - \tilde{d})\,\bar{d}/\tilde{d}$ denotes the localization exponent of the fractal structure. Note that this result agrees with the prediction of reference [27], obtained through a different argument. In figure 23 are shown some numerical results : $\Delta R/R$ *vs.* $\eta = a/L_\varphi$ at zero magnetic field. Clearly, the scaling behaviour (Eq. (69)) is well obeyed.

4.4.2 *Finite magnetic field.* — Following the scaling arguments of reference [25], one expects two different regimes

weak fields ($H\mathfrak{L}_\varphi^2 \ll \phi_0$) :

$$\Delta R/R(H = 0) - \Delta R/R(H) \sim H^2 \tag{70}$$

typical fields ($H\mathfrak{L}_\varphi^2 \gg \phi_0$) :

$$\Delta R/R(H) \sim H^{+\beta_L/2}. \tag{71}$$

Note that equations (70), (71) are simply the extension to fractals, of the known results on Euclidean networks (at $d = 2$, $\beta_L = 0$ and one gets the usual logarithmic regime). This behaviour is actually well observed on the numerical results shown in figure 24. The slope of $\Delta R/R$ *vs.* ϕ/ϕ_0 in a log-log plot is given by $\beta_L/2$.

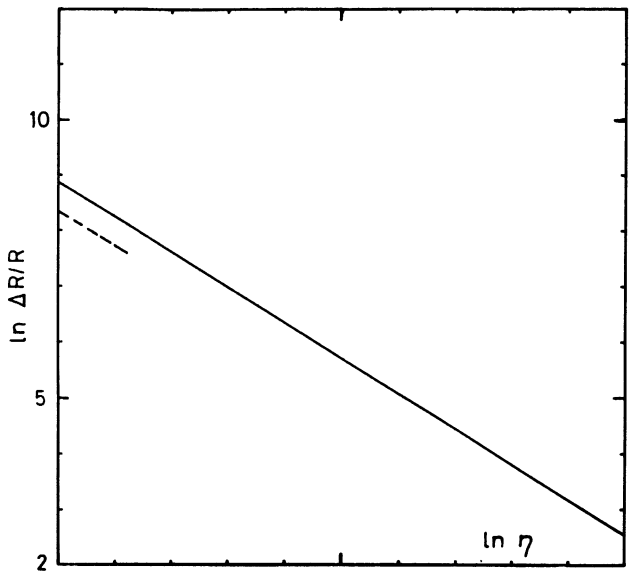

Fig. 23. — ln $\Delta R/R$ as a function of ln η for the Sierpinski gasket. The expression of $\Delta R/R$ (Eq. (C.1)) has been divided by η in order to take into account the L_φ dependence of the factor κ. For comparison, a dashed line of slope $\tilde{d} - 2 = \frac{2 \ln 3}{\ln 5} - 2 \simeq 0.6348$ is drawn. The scaling behaviour, equation (69) is well obeyed.

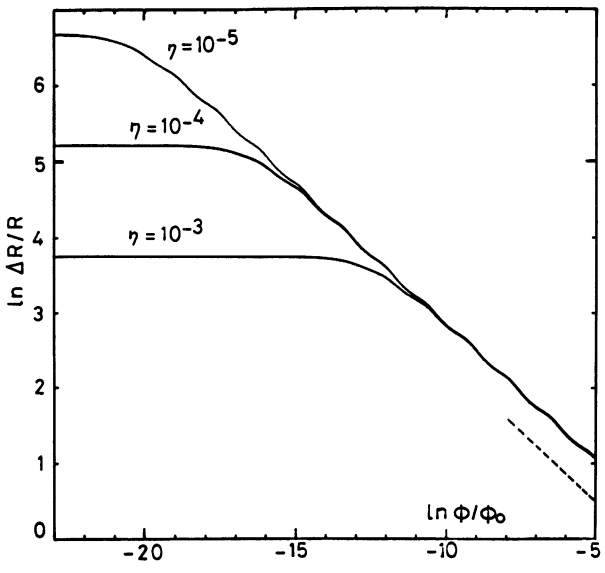

Fig. 24. — Log-log plot of $\Delta R/R$ as a function of the reduced flux ϕ/ϕ_0 through the elementary triangular cell of the Sierpinski gasket, for $\eta = 10^{-5}$, 10^{-4} and 10^{-3} respectively. The figure shows clearly the crossover between weak and large field regimes. The crossover field increases when L_φ decreases. In addition to the main power-like behaviour predicted by equation (71), one observes modulations of $\Delta R/R$, with a period of ln 4. The dashed line of slope $-\beta_L/2 = \tilde{d}(2 - \tilde{d})/2\,\tilde{d} \simeq 0.36848$ has been drawn for comparison.

However, the power law (Eq. (71)) so obtained is actually modulated by a small periodic function. The period of this oscillation is ln 4, i.e. the ratio of the areas of two consecutive triangles on the gasket. The physical origin of this phenomenon is the following. As was shown in Appendix C, the gasket breaks down into independent pieces after m^* iterations of the renormalization procedure. This gives rise to equation (69) in zero magnetic field. The magnetic field H controls actually this long range cut-off. Decreasing the magnetic field by a factor of four corresponds to an increase by a factor of two of the long range cut-off and this is equivalent to iterating one more step. Therefore, the obtained modulations are the consequence of the dilation invariance of the gasket only under a discrete subgroup of the dilation group. Therefore, we expect that this fine structure will disappear in random fractal structures such as the percolation clusters.

The scaling behaviour of equations (70), (71) can be derived in the present case using the formulation of Appendix C. Indeed, in strong field regime the long range cut-off is no longer given by $\mathcal{L}_\varphi$. We can then set $\mu \sim \lambda$ as if $\mathcal{L}_\varphi = \infty$, and then obtain :

$$\phi_n/\phi_{n=0} = 4^n\left(4 + 13\left(\frac{3}{20}\right)^n\right)\Big/17\,. \qquad (72)$$

The maximal modulations of $\Delta R/R$ are obtained for ϕ/ϕ_0 corresponding to integer values of the renormalized fluxes ϕ and ϕ. According to equation (72), ϕ_n is the same for : ($n \gg 1$) (ϕ, n) and ($\phi/4$, $n + 1$). This explains quantitatively the « period » ln 4 of the modulation.

At low magnetic fields, $\Delta R/R$ as given by equation (34), is controlled by the spectrum of the tight-binding model on the gasket. This problem, with obvious notations, can be written as

$$4\,x_i - \sum_j e^{-i\gamma_{ij}}\,x_j = \omega^2\,x_i \qquad (73)$$

ω^2 is actually an eigenvalue of equation (73). Therefore, equation (34) implies :

$$\Delta R/R \sim \sum_\omega \frac{1}{4(\cosh\,\eta - 1) + \omega^2} \qquad (74)$$

where $\eta = a/L_\varphi$. As was shown for the square network case, $\Delta R/R$ is dominated by the low energy modes in the spectrum. Let us denote by $\omega_e(H)$ the lower edge spectrum, and assume a power law form : $\omega_e(H) \sim H^s$ as for Euclidean networks. In the limit $\eta = a/L_\varphi \ll 1$, equation (74) reduces to

$$\frac{\Delta R}{R}(H = 0) - \frac{\Delta R}{R}(H) \simeq \int_0^{\omega_e(H)} d\omega\,\omega^{\tilde{d}-1}/(2\,\eta^2 + \omega^2) \qquad (75)$$

and then

$$\Delta R/R(H = 0) - \Delta R/R(H) \sim \text{Const.} - H^{s(\tilde{d}-2)}. \qquad (76)$$

However, in the regime where $H\mathcal{L}_\varphi^2 \gg 1$, the long range cut-off length is given by H and then $\Delta R/R(H)$ is only a function of H. Therefore, we obtain :

$$\Delta R/R(H) \sim H^{s(\tilde{d}-2)}. \quad (77)$$

The comparison with equation (71) leads to :

$$s = \bar{d}/2\,\tilde{d}. \quad (78)$$

For the Sierpinski gasket, $\bar{d} = \ln 3/\ln 2$ and $\tilde{d} = 2 \ln 3/\ln 5$, leading to $s = \dfrac{\ln 5}{4 \ln 2} = 0.580$. This detailed analysis of the gasket confirms the expected scaling laws for the weak-localization corrections in non Euclidean structures. These results are relevant for the experiments done on metal-insulator mixtures, close to the percolation threshold [28, 29].

5. Comparison with experimental data.

Presently, a certain number of experiments have been performed on multiconnected networks [3-5]. In order to make a close comparison with the weak-localization theory predictions, we should take into account three effects, which have been neglected in the previous sections.

The first one is the finite width of wires, which is responsible for the damping of the MR oscillations at large field : the backscattering loops are no longer around a very well defined flux.

The second one is the spin-orbit and spin-flip scatterings which are responsible for a change in both the sign and the magnitude of the MR oscillations [16]. The third effect is given by electron-electron interactions. Indeed, the mutual influence between impurity scattering and screened Coulomb interactions of electrons is known [30, 31] to give important corrections to the conductivity at low temperatures. In the multiconnected networks considered here, the interaction effects on the Cooper channel have to be taken into account, at least for high enough perpendicular magnetic fields : $eH > k_B T/D$. However in the available experiments, $L_T \equiv (\hbar D/k_B T)^{1/2}$ is very small when compared to L_φ. This allows a good distinction between weak localization effects at small fields and interaction effect at large fields [31]. Therefore, we will assume that $L_T \ll L_\varphi$ and then neglect here the interaction effects.

5.1 FINITE WIDTH OF WIRES. — The finite width of wires can be taken into account, through a simple renormalization of the phase coherence length, which becomes a quadratic function of the applied magnetic field [32] :

$$L_\varphi(H) = L_\varphi(H = 0)\left[1 + \frac{\pi^2}{3}\left(\frac{HwL_\varphi}{\phi_0}\right)^2\right]^{-1/2}. \quad (79)$$

Here w denotes the finite width of wires. The original calculation, leading to equation (79) has been performed for a single wire, in the limit of small enough magnetic fields. However, equation (79) is no longer valid when the magnetic flux through the area of a network node ($\sim w^2$) becomes of order $\sim \phi_0$: there the MR becomes sensitive to the detailed shape of the nodes and our approach cannot be used. But, this occurs at very high fields and equation (79) breaks down before such fields are reached. Actually equation (79) is a good approximation as long as : $HwL_\varphi/\phi_0 \lesssim 1$. We have checked numerically the renormalization of L_φ, by comparing the multistrip expression (Eq. (47)) with the single loop result after the renormalization of L_φ. The obtained results are very satisfactory, supporting the validity of equation (79), in the field interval of interest.

5.2 SPIN-ORBIT AND SPIN-FLIP SCATTERING. — The presence of these processes can be taken into account by separating the singlet and triplet contributions to the Cooperon [16]. The spin-orbit interaction affects only the triplet one. Formally, L_φ has to be replaced by a combination [10] of L_φ, L_{so} and L_s :

$$L_{\text{triplet}} = \left[L_\varphi^{-2} + \frac{4}{3}L_{so}^{-2} + \frac{2}{3}L_s^{-2}\right]^{-1/2}$$

$$L_{\text{singlet}} = [L_\varphi^{-2} + 2\,L_s^{-2}]^{-1/2}. \quad (80)$$

The resulting Cooperon is then given by [16] :

$$C = -\frac{1}{2}C_{\text{singlet}} + \frac{3}{2}C_{\text{triplet}} \quad (81)$$

where C_{singlet} and C_{triplet} are obtained as before by replacing L_φ by L_{singlet} and L_{triplet} respectively.

A quantitative comparison between the theoretical results and experimental data is shown in figure 25. The solid line corresponds to Cu, at $T = 133$ mK, in a honeycomb network geometry. Here the spin-orbit

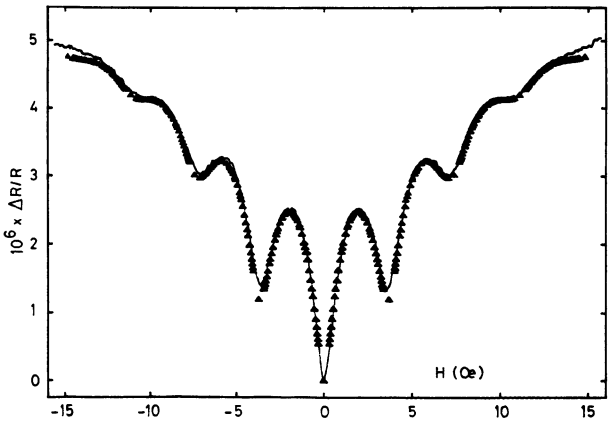

Fig. 25. — Quantitative comparison between the theoretical results (triangles) and experimental data (solid line), for Cu at $T = 133$ mK, taken from reference [3]. The hexagonal elementary cells (side $a = 1.5$ μm) are made of wires of width $w = 0.42$ μm. In this fit, we have $L_\varphi = 5.36$ μm and $L_{so} = 3.12$ μm respectively (L_{so} is the spin-orbit length).

coupling has been taken into account. In this situation the field renormalization of $\eta = a/L_\varphi$ gives

$$\eta^2(H) = \eta^2(H = 0) + \frac{4}{81}\pi^2(\phi/\phi_0)^2\,(w/a)^2 \qquad (82)$$

where ϕ denotes the magnetic flux through an elementary hexagonal cell (side a) made of wires of width w. This low-field approximation breaks down at $Haw \gtrsim \phi_0$. The renormalization of η becomes important at large H and is actually responsible for the damping of oscillations. Other experimental data [3] obtained for different metals, on square and honeycomb networks have also been analysed following the same scheme. This allowed in particular the calculation of the temperature variations of L_φ. The observed deviations, appearing at large H, have also been investigated. Detailed results will be given elsewhere [33].

Note that the results obtained on necklaces and ladders [4] also agree with our general results. For these geometries, a reduction of the MR oscillations has been found, in comparison with the single ring behaviour, when L_φ is large. Furthermore, the MR curve does not exhibit any fine structure in agreement with our conclusions.

6. Conclusions.

Our main results are summarized in the introduction. Let us conclude this paper with some remarks relative to our approach. The network formalism used in this paper assumes the validity of the Cooperon's equation (Eqs. (1), (2)) for the calculation of the magnetoresistance $\Delta R/R$ corrections. As can be seen, this approach gives a set of reliable results for extended networks as well as for the single ring [5] geometries. In this approach, all traces of randomness are summarized in the phase coherence length L_φ, and the theory is an averaged one [10]. In this respect, fluctuations from sample to sample are neglected and $\Delta\sigma(\mathbf{r})$ refers actually to an averaged correction to the conductivity. However recent numerical calculations, done on 1D ladders [35], suggest the existence of such fluctuations on the magnetoresistance behaviour. This problem of the probability distribution of the magnetoresistance is still open and some relevant results will reported in a forthcoming paper [35].

In addition to the self averaging question, the possibility of the coexistence of two harmonics (ϕ_0 and $2\,\phi_0$) has been raised recently [5, 18] on small systems. For instance, magnetoresistance oscillations with the expected period ϕ_0 have been observed recently [5] on thin-film rings (1-2 μm in diameter). This is the first observation in single rings of oscillations with flux period ϕ_0 at low fields. Small periodic oscillations (period $2\,\phi_0$) have also been observed at higher fields [5, 18] in such small systems. These results provide strong evidence that these two types of oscillations, seen on the same ring, arise from different interference mechanisms. Therefore, it is of importance to produce a unified theory for both types of oscillations using a single theoretical framework.

Acknowledgments.

The authors would like to thank Dr J. C. Angles d'Auriac and Dr B. Pannetier for friendly and useful discussions.

Appendix A.

Using the formalism developed in section 3, the matrix M for the single wire with N side branches, shown on figure 3a, can be written as

$$\begin{aligned}
M_{0,0} &= M_{N+1,N+1} = \coth(a/L_\varphi) \\
M_{i,i} &= 2\coth(a/L_\varphi) + \coth(b/L_\varphi), && 1 \leqslant i \leqslant N \\
M_{i',i'} &= \coth(b/L_\varphi), && 1 \leqslant i' \leqslant N \\
M_{i,i+1} &= 1/\sinh(a/L_\varphi), && 0 \leqslant i \leqslant N \\
M_{i,i'} &= 1/\sinh(b/L_\varphi), && 1 \leqslant i, i' \leqslant N .
\end{aligned}$$

The matrix M is a Jacobi-like one and then can be inverted recursively. The calculation of the cofactors T_{ii} of M can be done through the definition of the sequence $u_i = C_i/C_{i+1}$ giving the ratio of $C(x)$ at two successive nodes for the homogeneous equation. It is easy to show the following recursion equation for u_i's :

$$u_0 = 1/\cosh(a/L_\varphi)$$

$$u_{i+1} = \left[2\cosh\frac{a}{L_\varphi} + \tanh\frac{b}{L_\varphi}\sinh\frac{a}{L_\varphi} - u_i\right]^{-1} .$$

The coefficients T_{ii} can be expressed simply from the solution $\{u_i\}$:

$$\begin{aligned}
T_{0,0} &= T_{N+1,N+1} = \sinh(a/L_\varphi)/(\cosh(a/L_\varphi) - u_N), \\
T_{i,i} &= \sinh(a/L_\varphi)/[2\cosh(a/L_\varphi) + \tanh(b/L_\varphi)\sinh(a/L_\varphi) - u_{i-1} - u_{N-i}], && (1 \leqslant i \leqslant N) \\
T_{i,i+1} &= u_{N-i}\,T_{ii}, && (0 \leqslant i \leqslant N) \\
T_{i'i'} &= \tanh(b/L_\varphi) + T_{ii}/\cosh^2(b/L_\varphi), && (1 \leqslant i \leqslant N) \\
T_{i,i'} &= T_{ii}/\cosh(b/L_\varphi), && (1 \leqslant i \leqslant N)
\end{aligned}$$

The local correction to the conductivity is obtained from equation (30) and the above expressions for T_{ij}'s.

In order to calculate the global correction $\Delta R/R$, only the local correction along the principal axis of the wire has to be taken into account : current does not flow along the dandling branches. We obtain ($\eta = a/L_\varphi$) :

$$\frac{\Delta R}{R} = \frac{\kappa}{2}\left[\frac{\eta \cosh \eta - \sinh \eta}{\eta \sinh \eta} + \frac{2}{(N+1)}\left(\frac{\sinh \eta \cosh \eta - \eta}{\eta \sinh^2 \eta}\right)\sum_{\alpha=0}^{N} T_{\alpha\alpha} + \right.$$

$$\left. + \frac{2}{(N+1)}\,\frac{\eta \cosh \eta - \sinh \eta}{\eta \sinh^2 \eta}\sum_{\alpha=0}^{N} T_{\alpha,\alpha+1}\right].$$

In the limit $N \gg 1$, it is possible to simplify the result, replacing $T_{\alpha\alpha}$ by its limit :

$$u_\infty = \frac{1}{2}\left\{\left(2\cosh \eta + \tanh \frac{b}{L_\varphi} \sinh \eta\right) - \left[\left(2\cosh \eta + \tanh \frac{b}{L_\varphi} \sinh \eta\right)^2 - 4\right]^{1/2}\right\}$$

$$T_{\infty\infty} = \frac{\sinh \eta}{\left[\left(2\cosh \eta + \tanh \frac{b}{L_\varphi} \sinh \eta\right)^2 - 4\right]^{1/2}}.$$

Then

$$\frac{\Delta R}{R} = \frac{\kappa}{2\,\eta \sinh \eta}\left[\eta \cosh \eta - \sinh \eta + \frac{2[(\sinh \eta \cosh \eta - \eta) + (\eta \cosh \eta - \sinh \eta)\,u_\infty]}{\left[\left(2\cosh \eta + \tanh \frac{b}{L_\varphi} \sinh \eta\right)^2 - 4\right]^{1/2}}\right].$$

Note that for $b = 0$ we have $\frac{\Delta R}{R} = \frac{\kappa}{2}$, as is the case for an infinite wire.

Appendix B.

In this Appendix, we shall summarize some results relative to two networks, not discussed in the text, which can be of some experimental interest.

1) SINGLE RING WITH DANGLING SIDE BRANCHES (Fig. 26). — Let us denote by ϕ the magnetic flux through the loop (length = Na) and by b the common length of side branches. Using the notation of figure 26, one finds

$$C(x) = \frac{L_\varphi}{\hbar D S}\left(\sinh \frac{a}{L_\varphi} + \tanh \frac{b}{L_\varphi} \sinh \frac{x}{L_\varphi} \sinh \frac{a-x}{L_\varphi}\right) \cdot G$$

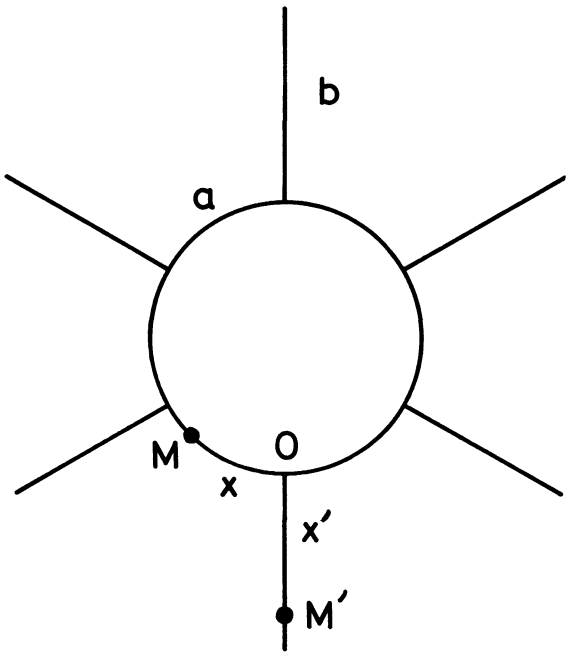

Fig. 26. — A closed ring geometry with dangling side branches.

for points x on the loop, and

$$C(x') = \frac{L_\varphi}{\hbar DS.\sinh b/L_\varphi}\left\{\sinh\frac{x'}{L_\varphi}\sinh\frac{b-x'}{L_\varphi} + \frac{\sinh^2 x'/L_\varphi}{\cosh b/L_\varphi} + \right.$$
$$\left. + G\cdot\frac{\sinh a/L_\varphi}{\sinh b/L_\varphi}\left[\frac{\sinh^2 x'/L_\varphi}{\cosh^2 b/L_\varphi} + \sinh^2\frac{b-x'}{L_\varphi} + 2\frac{\sinh x'/L_\varphi \sinh\dfrac{b-x'}{L_\varphi}}{\cosh b/L_\varphi}\right]\right\}$$

on a branch. Here G refers to the sum

$$G = \frac{1}{2N}\sum_{k=0}^{N-1}\left[\cosh\frac{a}{L_\varphi} + \frac{1}{2}\sinh\frac{a}{L_\varphi}\tanh\frac{b}{L_\varphi} - \cos\frac{2\pi}{N}\left(k + \frac{\phi}{\phi_0}\right)\right]^{-1}.$$

In practice, it is convenient to use the following compact expression for G :

$$G = (z^2-1)^{-1/2}(\alpha^N - \beta^N)\Big/\left(\alpha^N + \beta^N - 2\cos 2\pi\frac{\phi}{\phi_0}\right)$$

where

$$z = \cosh\frac{a}{L_\varphi} + \frac{1}{2}\sinh\frac{a}{L_\varphi}\tanh\frac{b}{L_\varphi}, \qquad \alpha = z + (z^2-1)^{-1/2}, \qquad \beta = z - (z^2-1)^{-1/2}.$$

Note that $C(x'=0) \leqslant C(x'=b)$ holds in general and the difference $C(x'=b) - C(x'=0)$ is larger at $\phi/\phi_0 = 1/2$ than at $\phi/\phi_0 = 0$.

2) CHAIN OF RINGS (Fig. 27). — For N identical rings, of length $2a$ each, articulated with identical strands (of length a each), the integrated correction to the total resistance R_{AB} is given by

$$\Delta R_{AB}/R_{AB} = \frac{\kappa}{2}\frac{1}{3N+1}\left\{(N-1)\frac{\eta\cosh\eta - \sinh\eta}{\eta\sinh\eta} + \frac{2\sinh\eta}{\cosh\eta - u_{2N+1}} + \right.$$
$$\left. + 6\sinh\eta\cdot\sum_{p=1}^{N}\left[3\cosh\eta - \left(u_{2p-1} + 2\cos\pi\frac{\phi}{\phi_0}\cdot u_{2(N-p)+2}\right)\right]^{-1}\right\}.$$

Here $\eta = a/L_\varphi$ and $\{u_p\}$ denotes the sequence, defined recursively by :

$$u_1 = 1/\cosh\eta$$
$$u_{2p} = 2\cos(\pi\phi/\phi_0)/(3\cosh\eta - u_{2p-1})$$
$$u_{2p+1} = 1/(3\cosh\eta - 2\cos(\pi\phi/\phi_0).u_{2p})$$

Appendix C.

In this appendix we shall outline the recursion procedure, used for the calculation of $\Delta R/R$ on the Sierpinski gasket. The notations are given in figure 22. The length L_φ refers to the bare coherence length. From equation (35), one has

$$\Delta R/R = \frac{\kappa}{4}\left\{\frac{\eta\cosh\eta - \sinh\eta}{\eta\sinh\eta} + \right.$$
$$\left. + 4\sinh\eta\frac{1}{N}\sum_i J_{ii}\right\}. \quad (C.1)$$

For convenience, we have replaced M by $\sinh\eta.M$.

The idea of the decimation procedure is the following. It is actually possible to express J_{AA}, J_{aa}, J_{AB}, ..., as functions of the inverse matrix elements J^R_{AA}, J^R_{BB}, J^R_{CC} of a renormalized operation J^R associated to the renormalized gasket (decimation by a factor 2). During this renormalization procedure, non diagonal matrix elements (e.a. J^R_{AB}) are introduced. At each step m of the recursion, $\Delta R/R$ is given as a linear combination of three gauge-invariant terms :

$$J(m) = \frac{1}{N_s(m)}\sum_\mu J^{(m)}_{\mu\mu}$$

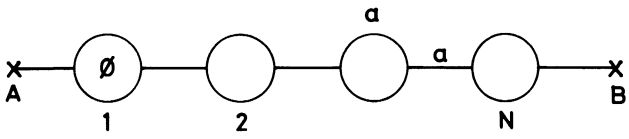

Fig. 27. — An open chain of rings with arms.

$$J_+(m) = \frac{1}{N_b(m)} \sum_{(\mu\nu)} J_{\mu\nu}^{(m)} \, e^{i\gamma_{\mu\nu}^{(m)}} \qquad (C.2)$$

and

$$J_-(m) = J_+^*(m) .$$

Here, $N_s(m)$ and $N_b(m)$ are respectively the number of sites and bonds of the gasket, at step m. The sum in $J_+(m)$ is taken over positively oriented bonds $(\mu\nu)$: the orientation of a bond is defined from that of the corresponding elementary triangle. The expression of $\Delta R/R$ can be written as

$$\Delta R/R = \frac{\kappa}{2} [X(m) + Y(m) J(m) + Z(m) J_+(m) + Z^*(m) J_-(m)]$$

where X, Y and Z are defined recursively (see below), and

$$X(0) = \frac{1}{2}(\eta \cosh \eta - \sinh \eta)/(\eta \sinh \eta)$$

$$Y(0) = 2 \sinh \eta , \quad Z(0) = 0 .$$

1) RENORMALIZATION OF THE OPERATOR M. — At step m, the matrix elements of the operator $M \equiv M^{(m)}$ are given by

$$M_{\mu\mu}^{(m)} = 4 \lambda_m \quad \text{and} \quad M_{\mu\nu}^{(m)} = - \mu_m \, e^{-i\gamma_{\mu\nu}}$$

(μ and ν connected by a single link). It is actually necessary to distinguish two effective fluxes through : corner triangles ϕ_m and central triangle $\bar{\phi}_m$. The recursion relations for λ_m, μ_m, ..., etc., can be written as

$$\lambda_{m+1} = \lambda - \frac{\mu^2}{\Delta} [16 \lambda^2 - \mu^2 + 4 \lambda\mu \cos 2\pi\phi + \mu^2 \cos 2\pi(\phi + \bar{\phi})]$$

$$[\mu \, e^{-i(y+z)}]_{m+1} = \mu_{m+1} \, e^{-i(y+z)} \, e^{i\theta} \qquad (C.3)$$

and

$$\mu_{m+1} \, e^{i\theta} = \frac{\mu^2}{\Delta} [16 \lambda^2 - \mu^2 + 4 \lambda\mu(e^{2i\pi(2\phi+\bar{\phi})} + 2 e^{2i\pi\phi}) + \mu^2(2 e^{2i\pi(\phi+\bar{\phi})} + e^{4i\pi\phi})] .$$

Here λ, μ, ϕ, $\bar{\phi}$, ... refer to λ_m, μ_m, ϕ_m, $\bar{\phi}_m$, ..., etc., at strep m. Δ is given by

$$\Delta = 64 \lambda^3 - 2 \mu^3 \cos 2\pi\bar{\phi} - 12 \lambda\mu^2 .$$

The phase factor θ is related to the reduced fluxes ϕ and $\bar{\phi}$ through :

$$\phi_{m+1} = 3 \phi_m + \bar{\phi}_m - \frac{3}{2\pi} \theta . \qquad (C.4)$$

Note that ϕ_m and $\bar{\phi}_m$ are related by $\phi_m + \bar{\phi}_m = 2.4^n \phi_{m=0}$. The set of equations (C.3) and (C.4) defines actually the new operator M, on the renormalized gasket.

2) RENORMALIZATION OF THE OPERATOR $J = M^{-1}$. — Using the renormalized operator M^R, one can write down the renormalization equations for $J(m)$, $J_+(m)$ and $J_-(m)$. Assume that we want to calculate J_{aa} for instance. J_{aa} is actually equal to x_a, where x_a, x_b, x_c, x_A, ..., are the solutions of the linear system associated to matrix M, the source term being located at node a. Therefore, in order to calculate J_{aa}, we start by calculating x_a, x_b and x_c as functions of x_A, x_B and x_C. The next step would be the calculation of x_A, x_B and x_C in terms of the inverse matrix $J^R = (M^R)^{-1}$. Coming back to x_a, x_b, x_c, one can deduce the desired quantities J_{aa}, J_{ab}, ..., etc. In order to perform such calculations, it is useful to introduce the 3×3 matrix D and the vector A :

$$\begin{bmatrix} J(m) \\ J(m) \\ J_-(m) \end{bmatrix} = D \begin{bmatrix} J(m+1) \\ J(m+1) \\ J_-(m+1) \end{bmatrix} + \begin{bmatrix} A(m) \\ A(m) \\ A_-(m) \end{bmatrix} .$$

The matrix elements of D are given by :

$$D_{11} = \frac{1}{3}\left[1 + \frac{2\mu^2}{\Delta^2}(2G + H e^{2i\pi\phi} + H^* e^{-2i\pi\phi})\right],$$

$$D_{12} = \frac{2}{3}\frac{\mu^2}{\Delta^2} e^{i\theta}[G + H e^{-2i\pi(2\phi+\bar{\phi})} + 2 H^* e^{-2i\pi\phi}],$$

$$D_{13} = D_{12}^* ,$$

$$D_{21} = \frac{2\mu}{3\Delta}[E + F e^{2i\pi\phi}] + \frac{\mu^2}{3\Delta^2}[G e^{2i\pi\phi} + H e^{-2i\pi(\phi+\bar{\phi})} + 2 H^*],$$

$$e^{-i\theta}.D_{22} = \frac{2\mu}{3\Delta}[E + F^* e^{-2i\pi\phi}] + \frac{\mu^2}{3\Delta^2}[G e^{-2i\pi(2\phi+\bar{\phi})} + 2 H e^{-2i\pi(\phi+\bar{\phi})} + H^*],$$

$$e^{i\theta}.D_{23} = \frac{2\mu}{3\Delta}[F e^{2i\pi\phi} + F^* e^{2i\pi(2\phi+\bar{\phi})}] + \frac{\mu^2}{3\Delta^2}[2 G e^{2i\pi\phi} + H e^{4i\pi\phi} + H^*],$$

$$D_{31} = D_{21}^* ; \qquad D_{32} = D_{23}^* ; \qquad D_{33} = D_{22}^* .$$

Here we have used the following notation :

$$E = 16\,\lambda^2 - \mu^2\,, \qquad F = 4\,\lambda\mu + \mu^2\,e^{i2\pi\bar{\phi}}$$
$$G = 256\,\lambda^4 + 3\,\mu^4 + 16\,\lambda\mu^3 \cos 2\,\pi\bar{\phi}$$
$$H = 128\,\mu\lambda^3 + 48\,\mu^2\,\lambda^2\,e^{2i\pi\bar{\phi}} + \mu^4(e^{-2i\pi\bar{\phi}} - 2\,e^{2i\pi\bar{\phi}})\,.$$

Similarly, the vector elements of A are given by

$$A(m) = \frac{2}{3\,\Delta}E; \qquad A_+(m) = \frac{1}{3\,\Delta}F^*\,, \qquad A_-(m) = \frac{1}{3\,\Delta}F\,.$$

Using the above notations, one deduces the recursion relations :

$$X(m+1) = X(m) + \frac{2}{3\,\Delta}E.Y(m) + \frac{1}{3\,\Delta}F^*.Z(m) + \frac{1}{3\,\Delta}F.Z^*(m)$$

$$\begin{bmatrix} Y(m+1) \\ Z(m+1) \\ Z^*(m+1) \end{bmatrix} = {}^tD \begin{bmatrix} Y(m) \\ Z(m) \\ Z^*(m) \end{bmatrix}\,.$$

Here ${}^tD$ denotes the transpose of the matrix D.

During the iteration, μ_m converges very rapidly towards zero. Therefore M can be approximated, after m^* iterations, by a diagonal matrix and this leads to : $\frac{\Delta R}{R} \simeq \frac{\kappa}{2}[X(m^*) + Y(m^*)/4\,\lambda_m^*]$.

References

[1] ALTSHULER, B. L., ARONOV, A. G. and SPIVAK, B. Z., *JETP Lett.* **33** (1981) 94.

[2] AHARONOV, Y. and BOHM, D., *Phys. Rev.* **115** (1959) 485.

[3] PANNETIER, B., CHAUSSY, J., RAMMAL, R. and GANDIT, P., *Phys. Rev. Lett.* **53** (1984) 718 ; *Phys. Rev.* **B 31** (1985) 3209.

[4] BISHOP, D. J., LICINI, J. C. and DOLAN, G. J., *Appl. Phys. Lett.* **46** (1985) 1000 ; AT and T. Bell Laboratories preprints (1985).

[5] CHANDRASEKHAR, V., ROOKS, M. J., WIND, S. and PROBER, D. E., *Phys. Rev. Lett.* **55** (1985) 1610.

[6] SHARVIN, D. Y. and SHARVIN, Y. V., *JETP Lett.* **34** (1981) 272.

[7] For a recent review, see SHARVIN, Y. V., *Physica* **126B-C** (1984) 288, and references to previous work therein.

[8] BRANDT, N. B., BOGACHEK, E. N., GITSU, D. V., GOGADZE, G. A., KULIK, I. O., NIKOLAEVA, A. A. and PONOMAREV, Y. G., *Sov. Phys. J. Low Temp. Phys.* **8** (1982) 358.

[9] LITTLE, W. A. and PARKS, R. D., *Phys. Rev. Lett.* **9** (1962) 9.

[10] KHMELNITSKII, D. E., *Physica* **126B-C** (1984) 235.
See also BERGMANN, G., *Phys. Reports* **107** (1984) 1.
LEE, P. A. and RAMAKRISHNAN, T. V., *Rev. Mod. Phys.* **57** (1985) 287.

[11] ALEXANDER, S., *Phys. Rev.* **B27** (1983) 1541.
RAMMAL, R., LUBENSKY, T. C. and TOULOUSE, G., *Phys. Rev.* **B 27** (1983) 2820.

[12] PANNETIER, B., CHAUSSY, J., RAMMAL, R. and VILLEGIER, J., *Phys. Rev. Lett.* **53** (1984) 1845.

[13] DOUCOT, B. and RAMMAL, R., *Phys. Rev.* **B** (1986). To be published.

[14] DOUCOT, B. and RAMMAL, R., *Phys. Rev. Lett.* **55** (1985) 1148.

[15] The first quantum correction to the conductivity is given by a series of diagrams which closely resemble the cooper-pair diagrams of Superconductivity theory and are called Cooperons.
See ANDERSON, P. W., *Physica* **117-118B** (1983) 30.

[16] ALTSHULER, B. L., ARONOV, A. G., KHMELNITSKII, D. E. and LARKIN, A. I., in *Quantum Theory of solids*, edited by I. M. Lifshitz (Izdatelstvo Mir, Moscou) 1982, p. 130.

[17] VOLKOV, V. A., *JETP Lett.* **36** (1982) 475.

[18] For recent theoretical works on small systems, see BUTTIKER, M., IMRY, Y., LANDAUER, R. and PINHAS, S., *Phys. Rev.* **B 31** (1985) 6207 and references therein.
Recent experimental work may be found in WEBB, R., WASHBURN, S., UMBACH, C. P. and LAIBOWITZ, R. B., *Phys. Rev. Lett.* **54** (1985) 2696.

[19] ALTSHULER, B. L., ARONOV, A. G. and ZYUZIN, A. Y., *Sov. Phys. JETP* **59** (1984) 415.

[20] See for instance HOFSTADTER, D. R., *Phys. Rev.* **B 14** (1976) 2239 and references therein.

[21] CLARO, F. and WANNIER, G. H., *Phys. Status Solidi* (b) **88** (1978) K147.

[22] RAMMAL, R., *J. Physique* **46** (1985) 1345.

[23] RAMMAL, R. and TOULOUSE, G., *Phys. Rev. Lett.* **49** (1982) 1194.

[24] BANAVAR, J. R., KADANOFF, L. P. and PRUISKEN, A. M. M., *Phys. Rev.* **B 31** (1985) 1388.

[25] KHMELNITSKII, D. E., *JETP Lett.* **32** (1980) 229.

[26] ALEXANDER, S. and ORBACH, R., *J. Physique Lett.* **43** (1982) L-625.
[27] RAMMAL, R. and TOULOUSE, G., *J. Physique Lett.* **44** (1983) L-13.
[28] ARONOV, A. G., GERSHENZON, M. E. and ZHURAVLEV, Y. E., *Sov. Phys. JETP* **60** (1984) 554.
[29] DEUTSCHER, G., GOLDMAN, A. M. and MICKLITZ, H., *Phys. Rev.* **B 31** (1985) 1679.
[30] FUKUYAMA, H., *J. Phys. Soc. Jpn.* **48** (1980) 2169.
[31] LIN, B. J. F., PAALANEN, M. A., GOSSARD, A. C. and TSUI, D. C., *Phys. Rev.* **B 29** (1984) 927.
[32] ALTSHULER, B. L. and ARONOV, A. G., *JETP Lett.* **33** (1981) 499.
[33] DOUCOT, B. and PANNETIER, B., *Phys. Rev.* **B** (1986). To be published.
[34] FOURCADE, B., preprint (1985).
[35] DOUCOT, B. and RAMMAL, R., submitted to *Phys. Rev. Lett.* (1986).